



**HAL**  
open science

## Climate change impact on sea surface winds in Southeast Asia

Marine Herrmann, Tung Nguyen-Duy, Thanh Ngo-Duc, Fredolin Tangang

► **To cite this version:**

Marine Herrmann, Tung Nguyen-Duy, Thanh Ngo-Duc, Fredolin Tangang. Climate change impact on sea surface winds in Southeast Asia. *International Journal of Climatology*, 2021, 42 (7), pp.3571-3595. 10.1002/joc.7433 . insu-04398191

**HAL Id: insu-04398191**

**<https://insu.hal.science/insu-04398191v1>**

Submitted on 10 Jul 2024

**HAL** is a multi-disciplinary open access archive for the deposit and dissemination of scientific research documents, whether they are published or not. The documents may come from teaching and research institutions in France or abroad, or from public or private research centers.

L'archive ouverte pluridisciplinaire **HAL**, est destinée au dépôt et à la diffusion de documents scientifiques de niveau recherche, publiés ou non, émanant des établissements d'enseignement et de recherche français ou étrangers, des laboratoires publics ou privés.

# Climate change impact on sea surface winds in Southeast Asia

Marine Herrmann<sup>1</sup>, Nguyen Duy Tung<sup>1</sup>, Thanh Ngo-Duc<sup>2</sup>, Fredolin Tangang<sup>3</sup>

<sup>1</sup> LEGOS, IRD, UMR556, IRD/CNES/CNRS/Université de Toulouse, 31400 Toulouse, France

<sup>2</sup> Department of Space and Applications, University of Science and Technology of Hanoi (USTH), Vietnam Academy of Science and Technology (VAST), 18 Hoang Quoc Viet, Cau Giay, Hanoi, Vietnam

<sup>3</sup> Department of Earth Sciences and Environment, Faculty of Science and Technology, Universiti Kebangsaan Malaysia, 43600 Bangi, Selangor, Malaysia

ORCID: Marine Herrmann 0000-0001-6125-7238; Thanh Ngo-Duc 0000-0003-1444-7498 ; Fredolin Tangang 0000-0002-4919-1800

Corresponding author: Marine Herrmann, marine.herrmann@ird.fr

Keywords: Southeast Asia; Climate Change; Sea surface wind; dynamical downscaling added value; regional climate model; ensemble simulations; CORDEX-SEA

**19 Abstract**

20 Numerical representation and climate projections of sea surface winds over Southeast  
21 Asia (SEA) are assessed here using an ensemble of the Coupled Model Intercomparison  
22 Project Phase 5 (CMIP5) downscaled simulations performed over the 20<sup>th</sup> and 21<sup>st</sup>  
23 centuries under Representative Concentration Pathways (RCPs) 4.5 and 8.5 scenarios  
24 within the CORDEX-SEA project. The ensemble is based on 2 Regional Climate  
25 Models (RCMs, RegCM4 and RCA4), and CMIP5 simulations performed with 5 Global  
26 Climate Models (GCMs : CNRM\_CM5, HadGEM2, GFDL, MPI-ESM-MR, EC-Earth).  
27 Comparison with QuikSCAT satellite data shows that dynamical downscaling improves  
28 sea surface wind speed representation, mainly by reducing its underestimation. The  
29 level of improvement depends on the RCM choice, GCM performance and wind  
30 strength.

31 Our results reveal significant differences in modeled projections of sea surface wind,  
32 depending on the models, RCPs, regions and season. GCMs simulate weak and  
33 contrasted changes, stronger for RCP8.5, with no clear common trend. RCA4 simulate  
34 weak changes, with high similarities between pairs, but contrasted results between  
35 RCPs. RegCM4 simulate stronger changes, with a weakening of average and intense  
36 winds for all seasons, stronger in June-August and in RCP8.5 than in RCP4.5. RCA4  
37 and RegCM4 simulate different changes, with no clear common trend except a  
38 weakening of seasonal and intense winds and an increase of seasonal wind interannual  
39 variability for June-August in RCP4.5, stronger for RegCM4. This corresponds to a  
40 weakening of the boreal summer monsoon and a slight increase of its interannual  
41 variability, and presumably to a decrease of the tropical cyclone frequency.

42 Differences of seasonal sea surface wind changes between models are related to  
43 differences of sea level pressure gradient changes. For a given RCM, those differences  
44 are partly related to the differences between parent GCMs. Finally, results suggest that  
45 uncertainties related to the RCM choice are larger than those related to the GCM choice.

Peer Review Only

## 1    **1    Introduction**

2    Southeast Asia (SEA) is submitted to a wide range of climate forcing: tropical cyclones  
3    (TC, Mei and Xie 2016), seasonal monsoons (Chang et al. 2005), interannual variability  
4    such as El Niño Southern Oscillation (ENSO, Juneng and Tangang 2005), climate  
5    change (Tangang et al. 2020). In this region with many coastal areas of huge population  
6    density (CIESIN, 2005), the question of climate change impact is crucial. The Southeast  
7    Asia Regional Climate Downscaling/Coordinated Regional Climate Downscaling  
8    EXperiment (SEACLID/CORDEX-SEA) group aims to improve the knowledge of this  
9    impact: regional climate models (RCMs, Tangang et al. 2018, 2019, 2020) were used to  
10    downscale several global climate models (GCMs) simulations of the Coupled Model  
11    Intercomparison Project Phase 5 (CMIP5) over SEA.

12  
13    Most downscaled climate projection studies in SEA focused on surface temperature and  
14    precipitation, showing spatiotemporally contrasted impacts (Ngo-Duc et al. 2014,  
15    Tangang et al. 2018, 2019, 2020, Trinh-Tuan et al. 2019, Supari et al. 2020). Several  
16    studies focused on TCs. Dynamical downscaling was shown to improve the  
17    representation of TC genesis and tracks over SEA (Diro et al. 2014; Wu et al. 2014), but  
18    underestimate their intensity and frequency, due to their resolution and coverage  
19    (Barcikowska et al. 2017, Gallo et al. 2018, Tibay et al. 2021 for RegCM3). Gallo et al.  
20    (2018) projected a tendency for fewer but slightly more intense TC over the Philippines.  
21    Dutheil et al. (2020) projected a decrease of cyclogenesis by half over South Pacific,  
22    attributed to a stronger vertical wind shear induced by a Convergence Zone equatorward  
23    shift. Examining the wind response to climate change is relevant for many aspects such

24 as risk, wind potential energy (Moemken et al. 2018, Soares et al. 2019, Chen et al.  
25 2020), oceans dynamics and ecosystems (Herrmann et al. 2013, 2014, Da et al. 2019,  
26 Piton et al. 2021). However, few studies focused on this question. Besides, though the  
27 added-value of dynamical downscaling in the representation of sea surface wind was  
28 highlighted for other regions (e.g. for the Mediterranean and Europe, Herrmann &  
29 Somot 2008, Herrmann et al. 2011, Moemken et al. 2018), it was barely assessed over  
30 SEA. Herrmann et al. (2020) examined sea surface wind response to climate change in  
31 SEA, from the climatological average to extreme events. They used a dynamical  
32 downscaling of CNRM-CM5 CMIP5 simulations performed with RegCM4 under the  
33 Representative Concentration Pathways (RCP) 4.5 and 8.5 scenarios. They showed the  
34 added-value of a RegCM4 downscaling of CNRM-CM5 in simulating sea surface winds  
35 in SEA, mostly related to a reduction of their underestimation. Moreover, their results  
36 suggested a significant summer weakening of sea surface wind at all time scales,  
37 associated with a monsoon weakening and a decrease by almost half of TC frequency.  
38 Those conclusions regarding the added-value of dynamical downscaling and the climate  
39 projection of sea surface wind over SEA were however only based on one GCM-RCM  
40 pair. The quantification of uncertainties in model representation and projections of sea  
41 surface wind speed through multi-model ensemble analysis is therefore necessary to  
42 improve our understanding of climate change impact over SEA (Tebaldi and Knutti,  
43 2007).

44

45 The objective of this study is to use a multi-model approach to contribute to better  
46 assess climate change impact on sea surface wind over SEA, and to explore the  
47 uncertainties related to the model choice. For that, we analyze 5 GCMs CMIP5

48 simulations and their downscalings performed with 2 RCMs in the framework of  
49 CORDEX-SEA. We first evaluate by comparison with satellite observations the ability  
50 of those runs to reproduce daily sea surface wind speed over SEA, and the added value  
51 of the dynamical downscaling depending on the RCMs and parent GCMs. We then  
52 examine the modelled evolution of sea surface wind speed between the end of 20th and  
53 21st centuries, from the climatological average to the daily values, in the GCMs, RCMs  
54 and in their ensemble means.

## 55 **2 Models and data**

### 56 **2.1 GCMs runs**

57 CMIP5 simulations from 5 GCMs were downscaled over SEA: CNRM\_CM5,  
58 HadGEM2, GFDL, MPI-ESM-MR, EC-Earth. Historical GCM simulations running from  
59 1850 to 2005 were forced with a time-evolving historic reconstruction of observed  
60 greenhouse gas (GHG) concentrations. Future GCM projection simulations were forced  
61 from 2006 until 2100 with specified GHG concentrations consistent with the medium  
62 RCP4.5 and high RCP8.5 scenarios. Table 1 provides the references and sources for those  
63 GCM simulations.

### 64 **2.2 Downscaled runs**

65 We analyze an ensemble of dynamically downscaled runs performed by 5 teams (see  
66 Table 1 for an overview) with 2 RCMs (RegCM4 and RCA4) at a 25 km horizontal  
67 resolution over the CORDEX-SEA domain (see Figure 1a). These simulations run over

68 the historical and future periods under RCP4.5 and RCP8.5 hypothesis. They use  
69 outputs from the 5 GCMs listed above as lateral and initial conditions.

70 RegCM4 is developed by the International Center for Theoretical Physics (Giorgi et al.  
71 2012). It was used to downscale the 5 GCMs. The Rossby Central regional Atmospheric  
72 model (RCA4) is developed at the Swedish Meteorological and Hydrological Institute  
73 (Strandberg et al. 2015). It was used to downscale 2 GCMs (CNRM\_CM5 and  
74 HadGEM2).

75 Configurations and parameterization schemes used for CORDEX-SEA RegCM4 and  
76 RCA4 runs are detailed in Tangang et al. (2019, 2020). No spectral nudging was used.  
77 Hereafter, RCM\_GCM refers to the downscaling of a given GCM performed with a  
78 given RCM (see Table 1). We analyze model outputs in the SEA domain (Figure 1). We  
79 also analyse sea surface winds over five  $\sim 3^\circ \times 3^\circ$  boxes located in the main regions of  
80 interest (IO, Indian Ocean; SCS, South China Sea; PAC, Pacific Ocean; INDO,  
81 Indonesian seas, Figure 1).

### 82 **2.3 Satellite observations**

83 We use QuikSCAT LEVEL 3 daily sea surface wind observations, available with a  
84  $0.25^\circ$  resolution from July 1999 to November 2009 on  
85 [https://podaac.jpl.nasa.gov/dataset/QSCAT\\_LEVEL\\_3\\_V2](https://podaac.jpl.nasa.gov/dataset/QSCAT_LEVEL_3_V2).

## 86 **3 Representation of sea surface wind speed**

87 We assess the ability of GCM and RCM\_GCM runs and of their respective ensemble  
88 means to represent the spatiotemporal variability of sea surface wind speed over SEA.

89 We examine the added value of the dynamical downscaling from daily to climatological  
90 scales. For that, we compare model outputs with QuikSCAT, following previous studies  
91 (e.g. Capps and Zender 2008, Winterfeldt et al. 2011). For each model, we average at  
92 each grid point the daily sea surface wind speed simulated by RCP4.5 and RCP8.5  
93 simulations for 2006-2008. We concatenate this averaged time series with the time  
94 series simulated by the historical simulation over 2000-2005, obtaining a time series  
95 that can be compared with QuikSCAT over 2000-2008. We also compute the ensemble  
96 means of time series obtained for the 5 GCMs, named ENS-GCM hereafter, and for the  
97 7 RCM\_GCM pairs, named ENS-RCM hereafter.

### 98 **3.1 Climatological mean to intense wind speed**

99 Figure 2 shows the quantile-quantile plot (QQplots) of models versus observations of  
100 the wind speed averaged over boxes B1-B5 for the GCMs, RCMs and their ensembles,  
101 and the relative difference of absolute biases. Climatological mean and 95th percentile  
102 (q95) biases are given in Table 2. Figures 3,4 show the maps of the ratio of RCM vs.  
103 GCM mean and q95 biases.

#### 104 **3.1.1 GCMs underestimation**

105 Most GCMs underestimate sea surface wind speed over the whole spectrum of values  
106 for all boxes (Figure 2 and Table 2). Mean and q95 SEA average biases are negative for  
107 all the GCMs, exceeding 10% for all GCMs except MPI. Average SEA biases in ENS-  
108 GCM are in the lower range of individual biases (-15% for the mean, -19% for q95).

109

110 Locally, we obtain positive biases only for MPI, mostly related to an overestimation of  
111 strong winds: QQ-plots are below the identity line for weak winds and above for strong  
112 winds (Figure 2b,c,d). Besides that, all GCMs mean and q95 biases are negative for all  
113 boxes: QQ-plots are below the identity line for the whole spectrum of wind speed  
114 values. This underestimation is stronger for EC-Earth: mean and q95 biases exceed -  
115 10% for 4 over 5 boxes, and even -20% for 2 boxes. GFDL and MPI show the best  
116 performances: mean biases are below -10% for 4 boxes and q95 biases are below -10%  
117 for all boxes. ENS-GCM mean biases are intermediate (weaker than -15%) and ENS-  
118 GCM q95 biases are in the lower range of individual runs biases (weaker than -11%).

### 119 **3.1.2 Downscaling added value**

120 The GCM underestimation of sea surface wind speed is globally reduced through the  
121 downscaling (Figures 2,3,4, Table 2). SEA average mean and q95 biases are strongly  
122 reduced for all the RCM\_GCM pairs. Bias reductions compared to the parent GCM  
123 exceed 10% for all pairs except RGM\_GFDL and RGM\_MPI.

124  
125 The stronger the underestimation by a GCM is, the more successful is the reduction by  
126 the downscaling. For EC-Earth, biases are reduced for all boxes for the mean, q95 and  
127 over most of the spectrum (Figure 2), and the improvement (reduction of bias) can  
128 exceed 15%. Mean and q95 SEA average biases are reduced in RGM\_EC compared to  
129 EC-Earth over respectively 81% (Figure 3) and 85% (Figure 4) of the SEA area. As a  
130 result, the mean bias in RGM\_EC is below 10% and the q95 bias below 5% for 3 boxes.  
131 For CNRM-CM5, the downscaling also reduces biases for all boxes. The improvement  
132 is slightly better with RegCM4 than with RCA4. In both RGM\_CNRM and

133 RCA\_CNRM, the mean bias is reduced for 4 over 5 boxes (by up to 15% in  
134 RGM\_CNRM and up to 12% in RCA\_CNRM). The q95 bias is reduced for all boxes  
135 (by up to 12% in both RCMs). Mean and q95 biases are reduced compared to CNRM-  
136 CM5 over respectively 74% and 92% of SEA in RGM\_CNRM, and respectively 79%  
137 and 84% in RCA\_CNRM. The resulting mean bias in RGM\_CNRM is below 10% for 4  
138 boxes and the q95 bias is below 5% for all boxes. For RCA\_CNRM, the resulting mean  
139 bias is below 10% and the q95 bias is below 5% for 3 boxes, but both biases exceed  
140 10% for 2 boxes.

141 For HadGEM2, the initial underestimation is less pronounced and the improvement  
142 induced by downscaling is smaller. RegCM4 also performs better than RCA4.  
143 RGM\_HadGEM significantly reduces the mean bias for 2 over 5 boxes and q95 bias for  
144 4 boxes, by less than 10%. It increases biases for B3 (+5% for the mean) over most of  
145 the wind spectrum (see biases difference, Figure 2c). For RCA\_HadGEM, biases for the  
146 mean and whole spectrum are either insignificantly changed, or even increased (see  
147 differences of absolute biases for B2,4, Figure 2,b,d). The mean and q95 biases are  
148 reduced respectively over 75% and 91% of SEA with RGM\_HadGEM, and respectively  
149 over 57% and 82% with RCA\_HadGEM. The resulting mean and q95 biases are below  
150 6% for 4 boxes for RGM\_HadGEM. For RCA\_HadGEM, the mean and q95 biases  
151 exceeds 10% for respectively 4 and 2 boxes.

152 GFDL and MPI show the best performances, and the improvement induced by the  
153 downscaling is the least significant. For RGM\_GFDL, the mean bias is slightly reduced  
154 for 2 boxes (by less than 6%) and increases for B2,3,4 (by up to 19%) over the whole  
155 spectrum (Figure 2b,c,d). The q95 bias is only reduced for B5 and slightly increases for  
156 the other boxes. For RGM\_MPI, the mean and q95 biases increase by more than 6% for

157 one box and are only slightly reduced for one box. The areas of improvement are  
158 smaller than those obtained for the other downscaled runs. However, the mean and q95  
159 biases are still reduced over more than half of SEA in both RGM\_GFDL (respectively  
160 59% and 74%) and RGM\_MPI (55% and 59%). For RGM\_GFDL the resulting bias  
161 (positive for almost all boxes and variables) is below 10% for both variables for 3  
162 boxes, and reaches 20% for 2 boxes. For RGM\_MPI, the resulting mean and q95 biases  
163 are respectively below 10% and 5% for 4 boxes.

164  
165 ENS-RCM also reduces the mean and q95 biases for all boxes compared to ENS-GCM,  
166 by up to ~10% (Table 2). SEA average biases are reduced by ~15% (Table 2), and  
167 biases are reduced over respectively 83% and 96% of SEA area (Figures 3,4).

168

### 169 **3.1.3 Intercomparison of downscaled runs**

170 Mean and q95 SEA average biases are below 10% for all the RCM\_GCM pairs (Table  
171 2). Only 3 RCMs produce slight overestimation: RGM\_CNRM for q95,  
172 RCA\_HadGEM for the mean and RGM\_GFDL for the mean and q95. Besides that,  
173 mean and q95 values are always underestimated. Locally, downscaled runs behave at a  
174 first order similarly, with comparable QQplots (Figure 2). Biases are overall below 10%  
175 (mean and q95, Table 2), but are however larger for some given pairs, boxes and scales.

176 First, for B5, an area of weak winds in the southern PAC (Figure 1bcd), the  
177 underestimation of average wind speed exceeds 10% for ENS-GCM and all GCMs  
178 except HadGEM2 (Table 2). This bias is reduced in all RCMs except RCM-MPI and in  
179 ENS-RCM, but the resulting bias is below 10% only for RGM\_HadGEM,

180 RCA\_HadGEM and RGM\_GFDL. Moreover, for all GCMs except HadGEM2, the  
181 underestimation of q95 values is smaller than the underestimation of the mean values  
182 (by at least 3%). Except for HadGEM downscalings, this is also the case for RCMs (by  
183 at least 8%). This decreasing underestimation with increasing wind speeds reflects a  
184 general overestimation of the daily variability in this region in most of the GCMs and  
185 RCMs.

186 Second, 3 pairs (RCA\_CNRM, RCA\_HadGEM and RGM\_GFDL) show higher and  
187 positive biases for areas of strong winds, in the northern SCS and PAC (Figure 1bcd).  
188 For B3 and B4, the 2 only boxes where q95 exceeds 13 m.s<sup>-1</sup> in QuikSCAT, QQ-plots  
189 are above the identity line for those 3 pairs, and positive biases increase with increasing  
190 wind speeds. Biases are above +7% while they are negative or below +4% for the 4  
191 other pairs. Those 3 pairs therefore particularly overestimate strong winds.

192 Last, for CNRM-CM5 and HadGEM2 downscaled runs used here, RCA4 overestimates  
193 more (or underestimates less) wind speeds than RegCM4. RCA4 indeed produces  
194 positive biases for 1 to 2 boxes more than RegCM4 and SEA average biases are up to  
195 6% more positive for RCA4 than for RegCM4 (Table 2).

196

197 ENS-RCM overall reduces the biases over the whole range of values compared to the 7  
198 individual RCM\_GCMs pairs. On SEA average, mean and q95 biases are below 5%,  
199 and ENS-RCM QQplot is close to the identity line for all boxes, with biases below 10%  
200 for the mean and q95. They are thus smaller than biases obtained for individual pairs,  
201 that can exceed 20%.

202

### 203 3.2 Seasonal cycle

204 To evaluate the representation of the seasonal cycle, we consider time series of monthly  
205 climatological averages of sea surface wind speed over 2000-2008 for each box and  
206 model (Figure 5). Table 3 shows the correlation coefficients between observed and  
207 modeled time series.

208

209 Except for EC-Earth for B2, all GCMs show highly significant correlations with  
210 observations (i.e. with a p-value  $< 0.01$ , corresponding to correlation coefficients  $>$   
211  $0.71$ ). Correlations exceed  $0.80$  for the 5 boxes for MPI, for 4 boxes for CNRM-CM5,  
212 and for 3 boxes for HadGEM2, GFDL and EC-Earth. For ENS-GCM, correlations vary  
213 between  $0.86$  and  $0.98$ , in the upper range of those obtained for individual runs or even  
214 higher. GCMs therefore reproduce well the monthly chronology of climatological sea  
215 surface wind speed.

216

217 Downscaling does not significantly improve the correlations compared to the GCMs,  
218 and rather tends to decrease them. In particular, except for RGM\_GFDL, the correlation  
219 decreases for B2 for all RCM\_GCM pairs by more than  $0.1$  and is not significant except  
220 for RGM\_MPI. For the other boxes, results differ depending on the GCMs and RCMs.  
221 RGM\_GFLD is the only downscaled run that shows slight improvement for the 5 boxes  
222 (up to  $+0.08$ ). Both CNRM-CM5 downscaling show correlations close to CNRM-CM5.  
223 RGM\_EC shows contrasted results: the correlation increases by at least  $0.05$  for 2  
224 boxes, and decreases by at least  $0.05$  for 2 boxes. RGM\_MPI decreases the correlation  
225 by more than  $0.05$  for 3 boxes, and HadGEM downscaling by more than  $0.10$ .

226 Except for B2, most pairs show highly significant correlations with observations, with  
227 modeled values in the range of observed values. RCA\_HADGEM however shows non-  
228 significant correlations for 4 boxes with a strong (40% to 100%) summer  
229 overestimation. RGM\_HADGEM also shows a non-significant correlation for B3 with a  
230 ~30% underestimation of winter values.

231 ENS-RCM improves the representation of the seasonal cycle compared to individual  
232 RCMs runs. Correlations are highly significant for all boxes, varying between 0.76 and  
233 0.96. ENS-RCM correlations are higher than for each of the 7 runs for B1 and B2, than  
234 for 6 runs for B3 and B4, and than for 5 runs for B5. Except for B2, ENS-RCM shows  
235 correlation very similar to those obtained for ENS-GCM.

236 As CMIP5 time series do not correspond to the actual chronology, the sequence of  
237 events, including extreme events, is different between simulations and observations. We  
238 therefore evaluate how monthly climatological cycle computed over 9 years may be  
239 affected by interannual variability. For that, we compute, for each GCM and point, the  
240 correlation and bias between the climatological monthly time series computed  
241 respectively over the periods 2000-2008 (9 years) and 1985-2004 (20 years). The  
242 correlation is always highly statistically significant (between 0.94 and 1.00) and the bias  
243 is negligible (=0.0%). The choice of the period of averaging does therefore not  
244 significantly impact our results. This conclusion agrees with Herrmann et al. 2020, who  
245 showed for RCM-CNRM that including years of extreme wind events in their analysis  
246 did not significantly modified their results concerning the average cycle as well as daily  
247 variability. Herrmann et al. (2011) also showed that computing QQ-plots over 1 or 9  
248 years of QuikSCAT data did not significantly change their results.

### 249 3.3 Spatial variability

250 To assess the representation of daily sea surface wind speed spatial variability, we  
251 compute for each run and both metric (mean, q95) the spatial centered root-mean-square  
252 difference (RMSD), standard deviation ratio (STDR) and spatial correlation coefficient  
253 between the modeled and observed sea surface wind speed fields (Taylor Diagram in  
254 Figure 6).

255  
256 STDR exceeds 1 for all GCMs for the mean and q95: all GCMs overestimate the spatial  
257 variability of sea surface wind speed, for climatological and intense values. For the  
258 mean, STDR varies between 1.2 and 1.4, RMSD between 0.6 and 0.9, and the  
259 correlation between 0.72 and 0.83. Scores in ENS-GCM are globally improved  
260 compared to individual GCM runs for the mean (1.2, 0.6 and 0.85 for respectively  
261 STDR, RMSD and correlation). For q95, STDR varies between 1.3 and 1.7, RMSD  
262 between 1.9 and 1.3, and the correlation between 0.60 and 0.72. ENS-GCM improves  
263 STDR (1.5) compared to 3 of the 5 individual runs. It improves RMSD (1.1) and the  
264 correlation (0.70) compared to 4 of the 5 individual runs.

265  
266 Again, STDR exceeds 1 for all RCMs pairs and both metrics. This corresponds to an  
267 overestimation of the spatial variability. For RGM\_CNRM the spatial correlation for the  
268 mean wind decreases by  $\sim 0.03$  compared to the GCM. For the 6 other pairs it increases  
269 (by up to 0.1 in RCA\_CNRM and RCA\_HadGEM). The spatial correlation for q95  
270 increases for the 7 pairs (by more than 0.15 for RCA4 runs).

271 Overall, RCMs performances can be classified following 3 “groups”: a 1<sup>st</sup> group of 4  
272 RegCM4 pairs (RGM\_CNRM, RGM\_HadGEM, RGM\_MPI, RGM\_EC), a 2<sup>nd</sup> group  
273 including only RGM\_GFDL, and a 3<sup>rd</sup> group with both RCA4 pairs. Performances in  
274 terms of STDR and RMSD are significantly better for the 1<sup>st</sup> group (respectively below  
275 1.3 and 0.8 for the mean and 1.4 and 1.1 for q95) than for the 2<sup>nd</sup> (intermediate) and 3<sup>rd</sup>  
276 groups (above 1.6 and 0.9 for the mean, and 2.0 and 1.3 for q95). Conversely, for the  
277 spatial correlation, the range is ~0.1 better for the 2<sup>nd</sup> and 3<sup>rd</sup> groups than for the 1<sup>st</sup>  
278 group. The 2<sup>nd</sup> and 3<sup>rd</sup> groups therefore better improve the spatial correlation, i.e. the  
279 representation of the spatial patterns. Doing so, they however increase the  
280 overestimation of the spatial variability compared to the 1<sup>st</sup> group. This is consistent  
281 with the analysis of QQplots and mean and q95 biases above (see 3.1.2.2), and with the  
282 RCM/GCM ratio (Figure 3). For RCA4 runs and RGM\_GFDL, the ratio is below -1 in  
283 the northern part ( $> 10^{\circ}\text{N}$ ) of the domain, a region of strong winds (Figure 1). They are  
284 underestimated in GCMs and overestimated in those 3 pairs. Ratio is above 1 in the  
285 equatorial part, a region of weak winds. They are underestimated in GCMs and (even  
286 more) in those 3 pairs. Overall, those 3 pairs therefore overestimate strong winds and  
287 underestimate weak winds.

288 Downscaling effect on spatial variability representation seems therefore more related to  
289 the RCM choice than to the GCM choice. Indeed, differences of RMSD, STDR and  
290 spatial correlation are much stronger between pairs with different RCMs and same  
291 GCM, than between pairs with same RCM but different GCMs. Only RGM\_GFDL  
292 shows significant differences compared to the 4 other RegCM4 runs.

293 ENS-RCM performances are average between the 3 groups. STDR, RMSD and  
294 correlation coefficient are equal to 1.3, 0.6 and 0.90 for the mean and 1.6, 1.0 and 0.79

295 for q95. ENS-RCM therefore improves the spatial correlation compared to ENS-GCM  
296 (by 0.05 and 0.09 respectively for the mean and q95). It slightly increases STDR and  
297 RMSD by  $\sim 0.1$  for both metrics.

298

299 This comparison with QuikSCAT data therefore confirms conclusions obtained for the  
300 Mediterranean (Herrmann et al. 2011). It shows that dynamical downscaling overall  
301 reduces the underestimation of the whole spectrum of sea surface wind speeds over  
302 most (from more than 50% to more than 90%) of SEA for the 5 GCMs and 2 RCMs  
303 analysed here, though at different levels. The improvement depends in particular on the  
304 RCM and on the GCM performance. RegCM4 performs slightly better than RCA4 for  
305 the runs examined here, and the improvement is better when underestimation is  
306 stronger. It is also more significant for intense winds. Downscaling also improves the  
307 representation of spatial variability. The improvement of spatial correlation is however  
308 associated for some RCMs (RCA4 pairs and RGM\_GFDL) to a strong overestimation  
309 of spatial variability, with an overestimation of high values and an underestimation of  
310 weak values. Last, downscaling does not significantly improve the representation of  
311 climatological monthly cycles for most of the models, and rather tends to worsen it for  
312 HadGEM2 downscalings.

313 This evaluation moreover shows that the representation of sea surface wind speed  
314 spatiotemporal variability is realistic in all pairs of RCM\_GCM. However some groups  
315 of pairs perform slightly better, depending on the metrics examined. The group of 4  
316 RegCM4 runs performs better in terms of biases than the second group of RCA4 runs  
317 and RGM\_GFDL. However, the second group performs better in terms of spatial  
318 correlation. Regarding the representation of sea surface wind speed in downscaled runs,

319 and for the GCMs and RCMs examined here, the RCM choice therefore seems to have a  
320 stronger impact than the GCM choice. This suggests that uncertainties related to the  
321 RCM choice are larger than those related to the GCM choice (though for one case  
322 (RGM\_GFDL) the GCM choice can induce differences of the same order).

323 Finally, for both GCMs and the RCMs ensembles, taking the ensemble average of all  
324 runs significantly improves the representation of sea surface wind speed compared to  
325 individual runs : it decreases both mean and intense values biases and increases the  
326 temporal correlation for the monthly cycle. The ensemble averaging does not have a  
327 physical meaning beyond the simple arithmetic operation. This bias reduction in the  
328 ensemble compared to the individual pairs can be attributed to the compensation of  
329 individual pair's biases. Some pairs indeed tend to globally overestimate wind speed  
330 values (RCA\_HadGEM and RGM\_GFDL) and others to underestimate (RGM\_MPI,  
331 RGM\_EC and RGM\_CNRM).

#### 332 **4 Impact of climate change**

333 To assess the impact of climate change on sea surface wind speed, we examine the  
334 differences between two 20-year periods: 2079-2098 (named FUT) and 1986-2005  
335 (named HIST). To illustrate the changes in terms of climatological average, interannual  
336 variability and intense daily events, we compute the maps of relative variations between  
337 HIST and FUT of the climatological average of daily sea surface wind speed, CVy (the  
338 ratio between standard deviation of annual mean and its climatological average) and  
339 q95. They are shown for RCP4.5 and RCP8.5, for the whole year, December-January  
340 (DJF) and June-August (JJA) and for the ensemble means of GCMs (ENS-GCM, Figure  
341 7), of RegCM4 (ENS-RGM, Figure 8) and of RCA4 (ENS-RCA, Figure 9). Maps for

342 individual runs are shown in supplementary materials (Figures SM1-SM6 for GCMs  
343 and SM7-SM12 for RCMs). Table 4 shows for the individual runs and their ensembles  
344 the relative changes between HIST and FUT of the SEA average mean and q95 values  
345 for the whole year, JJA and DJF.

#### 346 **4.1 Yearly and seasonal climatological winds**

347 All GCMs simulate SEA average changes of yearly wind speed lower than 2%, and  
348 varying from one GCM to another (Table 4). 4 models simulate decreases for RCP4.5, 3  
349 for RCP8.5. SEA average changes are slightly stronger for DJF and JJA (up to 5%).  
350 Those changes show a large spatial variability, with different areas of changes  
351 depending on the GCM, season and RCP (Figures SM1, SM2). Locally, variations  
352 hardly reach +/- 10% for RCP4.5, vs. +/- 20% for RCP8.5.

353 ENS-GCM mostly simulates non-significant SEA average changes. It only simulates for  
354 RCP8.5 a weak SEA increase for JJA and a weak SEA decrease for DJF ( $\leq 2\%$ , Table  
355 4). The JJA increase occurs over most of the domain (Figure 7), and the DJF decrease  
356 occurs mostly over IO, INDO and southern PAC. They locally reach +/- 10% and are  
357 simulated by at least 4 GCMs.

358

359 Downscaled simulations show different results depending on the RCM.

360 All RegCM4 runs simulate a weakening of yearly average wind that covers most of  
361 SEA (Figures SM7, SM8). Decrease is stronger (reaching -10% for RCP8.5 on SEA  
362 average) for RGM\_HadGEM and RGM\_GFDL, both locally and on SEA average  
363 (Table 4). For ENS-RGM, it reaches in RCP8.5 -7% on SEA average and locally -10%

364 over IO and INDO (Figure 8). For DJF, all RegCM4 runs simulate a weakening over  
365 southern SEA, a region of weak winds (Figure 1d). In ENS-RGM, it is below -5% on  
366 SEA average and locally reaches -20% in RCP8.5. For JJA, the decrease occurs over  
367 most of SEA and is stronger than for DJF for most RegCM4 runs, with a -7% average  
368 SEA decrease in RCP8.5 for ENS-RGM. All RegCM4 runs simulate JJA decreases in  
369 the INDO and IO, and at least 4 RegCM4 runs over the northern and southern PAC,  
370 reaching -10% in ENS-RGM. For all seasons, decreases are globally stronger in RCP8.5  
371 than RCP4.5, both on SEA average (see Table 4, ~ 2% to 3% stronger for RCP8.5 in  
372 ENS-RGM) and locally (Figure 8). Most RegCM4 runs thus simulate on average over  
373 SEA a climatological winds weakening, stronger for the whole year and JJA than for  
374 DJF, stronger for RCP8.5 than RCP4.5, and of intensity depending on the parent GCM.  
375

376 RCA4 runs simulate quite different changes. First, changes are much weaker, below 4%  
377 on SEA average and not exceeding  $\sim\pm 10\%$  locally (Table 4, Figures SM7, SM8).  
378 Second, for a given RCP, both RCA\_CNRM and RCA\_HadGEM simulate quite similar  
379 results (Figure 9, SM7, SM8). However, significant trends, stronger for JJA (reaching  
380 +4%) are only simulated for RCP8.5 (Table 4). Locally, changes are also consistent  
381 between RCA\_CNRM and RCA\_HadGEM, but contrasted between both RCPs. Both  
382 RCA4 pairs simulate for RCP4.5 a weak (<10%) decrease for the northern PAC for the  
383 whole year and JJA vs. a weak increase for RCP8.5.

#### 384 **4.2 Daily variability and intense events**

385 The daily standard deviation and 95th and 99th percentiles are used as indicators of the  
386 daily variability, intense events and extreme events. As shown in Herrmann et al.

387 (2020), their spatiotemporal patterns and trends are very similar (Figures not shown).  
388 We therefore only show here the q95 maps (Figures 7, 8, 9, SM3, SM4, SM9, SM10).  
389  
390 GCMs simulate contrasted q95 changes. There is no clear common trend except a  
391 decrease over SEA for the whole year and DJF, and an increase over northern PAC and  
392 SCS. They are simulated in 4 of 5 models and vary from ~5% to ~20% (Figures 7, SM3,  
393 SM4). Besides that, the 5 GCMs simulate different results and trends, both spatially and  
394 on SEA average. SEA average changes are below 5% for most runs (Table 4).  
395  
396 Nearly all RegCM4 pairs simulate decreases on SEA average for both RCPs and all  
397 seasons (year, DJF and JJA), that vary from pair to pair similarly as for the mean (Table  
398 4). Decrease are weak for RGM\_CNRM, RGM\_MPI and RGM\_EC, exceed -5% for  
399 RGM\_HadGEM and even -10% for RGM\_GFDL in RCP8.5. For ENS-RGM, they  
400 reach -7% in RCP8.5. Locally, they are associated in particular with a weakening of  
401 intense winds over the INDO, IO and southern PAC, for all the seasons, simulated for  
402 all pairs and both RCPs (Figures 8, SM9, SM10). At least 4 pairs also simulate a  
403 decrease over the northern PAC for the year and JJA. These local decreases reach -10%  
404 for RCP4.5 and -20% for RCP8.5 in ENS-RGM. Both RCPs simulate similar spatial  
405 patterns for a given parent GCM, however, changes, whether decreases or increases, are  
406 stronger for RCP8.5, reaching locally +/-30% (Figures 8, SM9, SM10).  
407  
408 RCA4 runs simulate weaker changes compared to RegCM4. Again, for a given RCP,  
409 RCA\_CNRM and RGM\_HadGEM results are similar, while both RCPs simulate

410 contrasted results. Locally, RCA4 simulates for the whole year a decrease for both  
411 RCPs over the southern IO, PAC and INDO and an increase over the SCS, which do not  
412 exceed +/-10%. However, RCP4.5 simulates a decrease over all the PAC, whereas  
413 RCP8.5 simulates a decrease over the central and northern PAC. For DJF, both RCA4  
414 pairs simulate for both RCPs a weak (<2%) strengthening of intense winds on SEA  
415 average (Table 4). It is mainly related to a strengthening in the northern SCS, PAC and  
416 IO, though both pairs and RCPs simulate a weakening in the INDO, southern PAC and  
417 IO (Figures 9, SM9, SM10). Those variations reach locally +/-10% for RCA\_HadGEM.  
418 Areas of strong variations are larger in RCP8.5. For JJA, the difference between both  
419 RCPs is even clearer. RCP4.5 simulates a weakening of intense winds over most of  
420 SEA, whereas RCP8.5 simulates a strengthening over most of the PAC and SCS. Those  
421 variations locally reach +/- 10% in both RCPs in ENS-RCA.

422

423 For all GCMs and RCMs considered here, trends simulated for q95 are therefore very  
424 similar to those simulated for the climatological mean. Changes for the mean value thus  
425 affect the whole spectrum, including intense and extreme events. Again, results for a  
426 given RCM but different parent GCMs are closer than results with a given GCM but  
427 different RCMs.

### 428 **4.3 Interannual variability of yearly and seasonal averages**

429 To examine the impact of climate change on the interannual variability, we show the  
430 maps of CVy in Figures 7, 8, 9, SM5, SM6, SM11, SM12.

431

432 For all GCMs, CVy changes are weak. On SEA average, there is no clear common  
433 trend. For each season and each RCP, at least 2 GCMs simulate increases and 2 GCMs  
434 simulate decreases (Table 4). For RCP8.5, changes are stronger for GFDL, exceeding -  
435 3% on SEA average for all seasons and locally reaching ~-20%. For the other GCMs  
436 and for RCP4.5, changes are very weak, below 3% and not exceeding +/-10% locally  
437 (Figures 7, SM5, SM6).

438

439 Changes are stronger for RCMs, both on SEA average and locally.

440 Except RGM\_GFDL which simulates CVy decreases reaching -10% in the southern  
441 SEA in DJF, all RegCM4 pairs simulate for the whole year and DJF, for both RCPs,  
442 weak (<2% on SEA average, Table 4) and spatially contrasted changes (Figures SM11,  
443 SM12), with no clear common and significant trend (Figure 8). CVy changes are  
444 stronger for JJA, reaching 4% on SEA average. At least 4 pairs and ENS-RGM simulate  
445 for both RCPs a strong decrease over the PAC, that locally reaches ~10%. Moreover  
446 RCP4.5 simulates a strong increase over the southern SCS and equatorial IO.

447

448 Both RCA4 pairs simulate for all seasons weak and spatially contrasted changes of  
449 CVy. They however simulate locally large areas of common trend sign (Figures  
450 9, SM11, SM12), and spatial patterns are very similar in RCP4.5 and RCP8.5. Common  
451 features are a weak (<5%) increase over the PAC and a weak decrease over southern  
452 SEA for all seasons. RCA\_CNRM simulates slightly stronger changes than  
453 RCA\_HadGEM, in particular in JJA, locally reaching +/-10%.

454

455 CVy changes in downscaled simulations are therefore strongly contrasted, depending on  
456 the season, region and RCM. There is practically no clear common signal. 6 over 7  
457 downscaled runs however simulate, for both RCPs, a weak increase over the PAC for  
458 the whole year and for DJF, and a more significant increase over the PAC for JJA, that  
459 locally reaches 10%.

460

## 461 **5 The role of pressure gradient**

462 Herrmann et al. (2020) showed that the changes of seasonal wind speed could be  
463 attributed to variations of the mean sea level pressure (MSLP) meridional gradient. We  
464 show for individual runs (Figure 10) and for the 3 ensembles (Figure 11) this gradient  
465 during HIST, and its variations between HIST and FUT.

466 MSLP meridional gradient changes explain sea surface wind speed changes simulated  
467 in each RCM and GCM run and ensemble, both on average and spatially (Figures SM1,  
468 SM2, SM7, SM8 and Table 4). For example, MPI simulates over the whole range of  
469 latitude a strengthening of the negative meridional MSLP gradient in JJA, stronger in  
470 RCP8.5 than RCP4.5 (Figure 10). This is consistent with the strengthening of southward  
471 (Figure 1) wind simulated over all SEA (Figures SM1,SM2). HadGEM2 and  
472 RGM\_HadGEM simulates in JJA for RCP4.5 a MSLP meridional gradient weakening  
473 between 0°N and 20°N. This is consistent with the wind weakening simulated over this  
474 region. They simulate in DJF a MSLP gradient weakening (strengthening) south (north)  
475 of ~12°N, stronger in RCP8.5 than RCP4.5 in HadGEM. It is again consistent with the  
476 wind changes obtained over these ranges of latitude. These are some examples, but a

477 careful examination of Figures 10 and SM1, SM2 ,SM7, SM8 shows that those  
478 conclusions stand for all the runs.

479 MSLP meridional gradient changes (Figure 11) moreover explain the different sea  
480 surface wind speed trends obtained for the 3 ensembles. ENS-GCM simulates for DJF a  
481 MSLP gradient weakening (strengthening) south (north) of  $\sim 12^{\circ}\text{N}$ , consistent with  
482 corresponding wind speed changes (Figures 7, Table 4). It simulates for JJA an overall  
483 MSLP gradient strengthening consistent with the general SEA wind strengthening. Both  
484 MSLP gradient and wind speed changes are stronger in RCP8.5. ENS-RGM simulates  
485 both for DJF and JJA an overall MSLP gradient weakening, stronger in RCP8.5,  
486 consistent with the average SEA wind weakening (Figure 8). ENS-RCA simulates for  
487 DJF a MSLP gradient strengthening north of  $10^{\circ}\text{N}$ , stronger in RCP8.5, also consistent  
488 with the simulated wind changes (Figure 9). It simulates for JJA a MSLP gradient  
489 weakening (strengthening) for RCP4.5 (RCP8.5), again consistent with the RCP  
490 contrasted wind speed changes detailed in 4.1.

491 Finally, for a given RCM, differences between RCM\_GCM pairs are partly related to  
492 differences between parent GCMs, though it is not the only driver. For RGM\_GCM  
493 pairs (except RGM\_GFDL for RCP8.5), changes of yearly and seasonal average winds  
494 are indeed correlated with changes obtained in the parent GCM, as shown in Figure 12.  
495 This is related to the fact that (except for RGM\_GFDL with RCP8.5) MSLP meridional  
496 gradient changes in RegCM4 runs are also linked with MSLP changes in the parent  
497 GCM runs, as can be seen in Figure 10a,b.

498

## 499 **Conclusion**

500 This analysis is the first multi-model study focusing on the regional modeling and  
501 climate projection of sea surface wind speed in SEA.

502

503 Comparisons with QuikSCAT data confirm that dynamical downscaling of GCM  
504 simulations overall improves the representation of sea surface wind speed at all time  
505 scales, mainly by reducing its underestimation over most of SEA, for both RCMs  
506 considered here. It moreover shows that the level of improvements depends on the  
507 GCM, RCM and wind intensity. RegCM4 better reduces the underestimation while  
508 RCA4 better represents the spatial variability. The improvement is better for GCMs  
509 showing strong underestimation, and for strong winds. For both GCM and RCM  
510 ensembles, taking the ensemble average of all runs improves the representation of sea  
511 surface wind spatial and temporal variability, at all time scales compared to individual  
512 runs. This is presumably due to a bias compensation induced by arithmetic averaging.

513

514 Our results reveal significant differences in modeled projections of sea surface wind  
515 evolution, depending on the models, RCPs, regions and seasons. The 5 GCMs all  
516 simulate relatively weak and different changes. They are slightly stronger for RCP8.5  
517 than for RCP4.5, both spatially and on SEA average. There is no clear common trend  
518 other than a small weakening of average and intense winds in the southern IO in DJF for  
519 RCP8.5. RCA4 pairs also simulate weak changes, with strong similarities between both  
520 pairs, but contrasted results between RCPs. For RCP8.5, RCA4 simulates a  
521 strengthening of average and intense winds over most of SEA for all seasons. For

522 RCP4.5, it simulates a weakening for the whole year and JJA, and a slight strengthening  
523 for DJF. CVy changes in GCMs and RCA4 runs are overall weak and non-significant.  
524 RegCM4 runs and ensemble simulate more significant changes. First, they simulate  
525 over most of SEA a weakening of average and intense winds for all seasons and both  
526 RCPs. It locally reaches -20%, and is stronger for the whole year and JJA than for DJF,  
527 and stronger in RCP8.5 than in RCP4.5. The DJF weakening affects mostly the southern  
528 IO and PAC. The JJA weakening affects predominantly the southern SCS and northern  
529 PAC and all the southern SEA. Second, most RegCM4 runs simulate for JJA a CVy  
530 increase over the PAC that locally reaches 10% in RGM-ENS for RCP8.5. For both  
531 average and intense wind values, RCA4 and RegCM4 ensembles therefore simulate  
532 different changes, with no clear common trend between both ensembles except for JJA  
533 in RCP4.5: both ensembles simulate a weakening of average and intense winds and an  
534 increase of average wind interannual variability. It is stronger for RegCM4 and mainly  
535 located over the INDO, northern PAC and southern SCS.

536

537 These JJA climatological decrease and CVy increase correspond to a weakening of the  
538 intensity and increase of the interannual variability of boreal summer southerly  
539 monsoon. Climatological seasonal sea surface wind speed changes are related to MSLP  
540 meridional gradient changes, both for RCMs and GCMs. Factors inducing those MSLP  
541 gradient changes need further investigation to be understood in details. In particular  
542 factors inducing the stronger weakening of the gradient (and summer wind) simulated  
543 by RegCM4 than by GCM and RCA4 could also explain the results obtained by  
544 Tangang et al. (2020), who showed that RegCM4 projected a higher rainfall reduction  
545 than the parent GCMs. As shown by Herrmann et al. (2020), the intense winds

546 weakening in these regions and periods of strong TC activity presumably corresponds to  
547 a decrease of TC frequency. For comparable q95 decreases, they obtained a decrease by  
548 nearly half of yearly TC frequency. The present multi-model study therefore agrees with  
549 previous results (Gallo et al. 2018, Dutheil et al. 2020) suggesting that climate change  
550 could induce a weakening of TC activity over SEA.

551

552 This study partially sampled the uncertainties in terms of modeling and climate  
553 projections of sea surface wind speed associated with the RCM and GCM choices. It  
554 suggests, for the 5 GCMs and 2 RCMs examined here, that uncertainties related to the  
555 RCM choice are larger than those related to the GCM choice. Our conclusions are  
556 indeed partly related to the RCM choice. This underlines the need to run more  
557 downscaling experiments, varying in particular the number of RCMs. For a given RCM,  
558 differences between RCM\_GCM pairs are then partly related to differences between  
559 parent GCMs, though it is not the only driver. Further developments are necessary to  
560 increase the quality and robustness of downscaled projections (Giorgi, 2019). In  
561 particular, ocean-atmosphere regional coupling would be particularly relevant in this  
562 region of strong air-sea interactions. Moreover, the representation and projection of sea  
563 surface winds may now also be examined using coupled high resolution global  
564 simulations available through HighResMIP (Haarsma et al. 2016). Those simulations  
565 should reproduce better TCs but also Madden-Julian Oscillation (MJO, Hung et al.,  
566 2013, Ahn et al. 2017), both factors involved in seas surface wind extremes. The  
567 representation and climate projections in CORDEX-SEA downscaled simulations of  
568 MJO and TCs now require a more detailed examination based in particular on TC  
569 tracking tools, as done for 3 RegCM4 pairs by Tibay et al. (2021).

570 **Acknowledgements**

571 This work is part of LOTUS international joint laboratory (lotus.usth.edu.vn, IRD  
572 funding) and SEACLID/CORDEX-SEA Project (APN funding, ARCP2015-04CMY-  
573 Tangang). TND is supported by Vietnam National Foundation for Science and  
574 Technology Development (NAFOSTED) Grant 105.06-2018.05 and FTangang by  
575 Malaysian MOHE Funding Grant FRGS/1/2017/WAB05/UKM/01/2 and UKM  
576 Research University Grant GUP-2019-035. We thank CORDEX-SEA teams (AMU,  
577 RU-CORE, SMHI, UKM, USTH) for running the downscaled experiments.

578

579 **References**

580 Ahn, MS., Kim, D., Sperber, K.R. Kang, I. S., Maloney, E., Waliser, D. Hendon, H. on  
581 behalf of WGNE MJO Task Force. MJO simulation in CMIP5 climate models: MJO  
582 skill metrics and process-oriented diagnosis. *Clim Dyn* 49, 4023–4045 (2017).  
583 <https://doi.org/10.1007/s00382-017-3558-4>

584 Barcikowska, M., Feser, F., Zhang, W., & Mei, W. (2017). Changes in intense tropical  
585 cyclone activity for the western North Pacific during the last decades derived from a  
586 regional climate model simulation. *Climate Dynamics*, 49(9–10), 2931–2949.  
587 <https://doi.org/10.1007/s00382-016-3420-0>

588 Capps, S. B. and Zender, C. S. Observed and CAM3 GCM Sea Surface Wind Speed  
589 Distributions: Characterization, Comparison, and Bias Reduction, *Journal of Climate*,  
590 21(24), 2008, doi: 10.1175/2008JCLI2374.1

- 591 Center for International Earth Science Information Network - CIESIN - Columbia  
592 University, United Nations Food and Agriculture Programme - FAO, and Centro  
593 Internacional de Agricultura Tropical - CIAT (2005). Gridded Population of the World,  
594 Version 3 (GPWv3): Population Count Grid. Palisades, NY: NASA Socioeconomic  
595 Data and Applications Center (SEDAC). <http://dx.doi.org/10.7927/H4639MPP>
- 596 Chang C-P, Wang Z, McBride J, Liu C-H (2005) Annual Cycle of Southeast Asia—  
597 Maritime Continent Rainfall and the Asymmetric Monsoon Transition. *J. Clim.*, 18,287-  
598 301 doi:10.1175/jcli-3257.1
- 599 Chen, 2020, Impacts of climate change on wind resources over North America based on  
600 NA-CORDEX, Renewable Energy, <https://doi.org/10.1016/j.renene.2020.02.090>
- 601 Da, N. D., M. Herrmann, R. Morrow, R. Niño, N. M. Huan, & N. Q. Trinh (2019)  
602 Contributions of wind, eddies, chaotic variability and ENSO to the interannual  
603 variability of the South Vietnam Upwelling. *J. Geophys. Res.*,  
604 <https://doi.org/10.1029/2018JC014647>
- 605 Diro, G. T., Giorgi, F., Fuentes-Franco, R., Walsh, K. J. E., Giuliani, G., & Coppola, E.  
606 (2014). Tropical cyclones in a regional climate change projection with RegCM4 over  
607 the CORDEX Central America domain. *Climatic Change*, 125(1), 79–94.  
608 <https://doi.org/10.1007/s10584-014-1155-7>
- 609 Dutheil, C., Lengaigne, M., Bador, M. et al. (2020) Impact of projected sea surface  
610 temperature biases on tropical cyclones projections in the South Pacific. *Sci.*  
611 *Rep.*, **10**, 4838 <https://doi.org/10.1038/s41598-020-61570-6>
- 612 Gallo, F., Daron, J., Macadam, I., Cinco, T., Marcelino, I., Ii, V., ... Jones, R. G. (2018).  
613 High-resolution regional climate model projections of future tropical cyclone activity in

614 the Philippines: High-res. projections of future TC activity in the Philippines.  
615 International Journal of Climatology, (March), 1–14. <https://doi.org/10.1002/joc.5870>

616 Giorgi F, Coppola E, Solmon F, Mariotti L, Sylla M, Bi X, Elguindi N, Diro G, Nair V,  
617 Giuliani G, Turuncoglu U, Cozzini S, Guttler I, O'Brien T, Tawfik A, Shalaby A, Zakey  
618 A, Steiner A, Stordal F, Sloan L, & Brankovic C. (2012) RegCM4: model description  
619 and preliminary tests over multiple CORDEX domains. *Clim. Res.*, **52**, 7–29,  
620 <https://doi.org/10.3354/cr01018>

621 Giorgi, F. (2019) Thirty years of regional climate modeling: Where are we and where  
622 are we going next? *Journal of Geophysical Research: Atmospheres*, **124**, [https://doi.org/](https://doi.org/10.1029/2018JD030094)  
623 [10.1029/2018JD030094](https://doi.org/10.1029/2018JD030094)

624 Haarsma, R. J., Roberts, M. J., Vidale, P. L., Senior, C. A., Bellucci, A., Bao, Q.,  
625 Chang, P., Corti, S., Fučkar, N. S., Guemas, V., von Hardenberg, J., Hazeleger, W.,  
626 Kodama, C., Koenigk, T., Leung, L. R., Lu, J., Luo, J.-J., Mao, J., Mizielinski, M. S.,  
627 Mizuta, R., Nobre, P., Satoh, M., Scoccimarro, E., Semmler, T., Small, J., and von  
628 Storch, J.-S. High Resolution Model Intercomparison Project (HighResMIP v1.0) for  
629 CMIP6, *Geosci. Model Dev.*, **9**, 4185-4208, doi:10.5194/gmd-9-4185-2016, 2016

630 Herrmann, M., C. Estournel, F. Adloff, & F. Diaz (2014) Impact of climate change on  
631 the northwestern Mediterranean Sea pelagic planktonic ecosystem and associated  
632 carbon cycle. *J. Geophys. Res.*, **119**, 5815-5836, <https://doi.org/10.1002/2014JC010016>

633 Herrmann, M., F. Diaz, C. Estournel, P. Marsaleix, & C. Ulses (2013) Impact of  
634 atmospheric and oceanic interannual variability on the Northwestern Mediterranean Sea  
635 pelagic planktonic ecosystem and associated carbon cycle. *J. Geophys. Res.*, **118**, 1–  
636 22, <https://doi.org/10.1002/jgrc.20405>

- 637 Herrmann, M., Ngo-Duc, T., & Trinh-Tuan, L. (2020) Impact of climate change on sea  
638 surface wind in Southeast Asia, from climatological average to extreme events: results  
639 from a dynamical downscaling. *Clim. Dyn.* **54**, 2101–2134,  
640 <https://doi.org/10.1007/s00382-019-05103-6>
- 641 Herrmann, M., S. Somot, S. Calmanti, C. Dubois, and F. Sevault (2011). Representation  
642 of wind variability and intense wind events over the Mediterranean sea using dynamical  
643 downscaling: impact of the regional climate model configuration. *NHESS*, 11, 1983-  
644 2001, 2011, doi:10.5194/nhess-11-1983-2011
- 645 Herrmann, M. and S. Somot (2008). Relevance of ERA40 dynamical downscaling for  
646 modeling deep convection in the North-Western Mediterranean Sea. *Geophys. Res.*  
647 *Let.*, 35, L04607, <http://dx.doi.org/10.1029/2007GL032442>
- 648 Hung, M.-P., J.-L. Lin, W. Wang, D. Kim, T. Shinoda, and S. J. Weaver (2013), MJO  
649 and convectively coupled equatorial waves simulated by CMIP5 climate models, *J.*  
650 *Clim.*, 26, 6185–6214.
- 651 Juneng L, Tangang FT (2005) Evolution of ENSO-related rainfall anomalies in  
652 Southeast Asia region and its relationship with atmosphere–ocean variations in Indo-  
653 Pacific sector. *Clim. Dyn.*, **25**, 337-350 <https://doi.org/10.1007/s00382-005-0031-6>
- 654 Mei, W., Xie, S. Intensification of landfalling typhoons over the northwest Pacific since  
655 the late 1970s. *Nature Geosci* 9, 753–757 (2016). <https://doi.org/10.1038/ngeo2792>
- 656 Moemken J., M. Reyers, H. Feldmann and J. G. Pinto, 2018, Future Changes of Wind  
657 Speed and Wind Energy Potentials in EURO-CORDEX Ensemble Simulations, *JGR-A*,  
658 10.1029/2018JD028473

- 659 Ngo-Duc, T., Kieu, C., Thatcher, M., Nguyen-Le, D., & Phan-Van, T. (2014) Climate  
660 projections for Vietnam based on regional climate models. *Clim. Res.*, **60**, 199-213.  
661 <https://doi.org/10.3354/cr01234>
- 662 Piton, V., M. Herrmann, P. Marsaleix, T. Duhaut, Trinh Bich Ngoc, Manh Cuong Tran,  
663 K. Shearman, S. Ouillon (2021). Influence of winds, geostrophy and typhoons on the  
664 seasonal variability of the circulation in the Gulf of Tonkin: A high-resolution 3D  
665 regional modeling study, *Regional Studies in Marine Science*, 45,  
666 101849, <https://doi.org/10.1016/j.rsma.2021.101849>
- 667 Soares, P. M. M., D. C. A. Lima, A. Semedo, W. Cabos and D. V. Sein, 2019, Climate  
668 change impact on Northwestern African offshore wind energy resources, *Environ. Res.*  
669 *Lett.*, <https://doi.org/10.1088/1748-9326/ab5731>
- 670 Strandberg, G., Barring, L., Hansson, U., Jansson, C., Jones, C., Kjellström, E., Kolax,  
671 M., Kupiainen, M., Nikulin, G., Samuelsson, P., Ullerstig, A., Wang, S. (2015)  
672 CORDEX scenarios for Europe from the Rossby Centre regional climate model RCA4.  
673 *Rep. Meteorol. Climatol.* 116, 84, ISSN: 0347-2116
- 674 Supari, S., L. Juneng, F. Cruz, J.X. Chung, S.T. Ngai, E. Salimun, M.S.F. Mohd, J.  
675 Santisirisomboon, P. Singhruck, P.V. Tan, T. Ngo-Duc, G. Narisma, E. Aldrian, D.  
676 Gunawan, & A. Sopaheluwakan (2020). Multi-model Projections of Precipitation  
677 Extremes in Southeast Asia based on CORDEX-Southeast Asia simulations.  
678 *Environmental Research*, **184**, 109350, <https://doi.org/10.1016/j.envres.2020.109350>
- 679 Tangang, F., J. X. Chung, L. Juneng, Supari, E. Salimun, S. T. Ngai, A. F. Jamaluddin,  
680 M. S. Faisal, F. Cruz, G. T. Narisma, J. Santisirisomboon, T. Ngo-Duc, V. T. Phan, P.  
681 Singhruck, D. Gunawan, E. Aldrian, A. Sopaheluwakan, G. Nikulin, A. R. C. Remedio,

- 682 D. V. Sein, D. Hein-Griggs, and J. L. McGregor, 2020: Projected Future Changes in  
683 Rainfall in Southeast Asia based on CORDEX – SEA Multi-model Simulations.  
684 *Climate Dyn.*, 55(5), 1247-1267 <https://doi.org/10.1007/s00382-020-05322-2>
- 685 Tangang, F., Je. Santisirisomboon, L. Juneng, E. Salimun, J. Chung, Supari, F. Cruz, T.  
686 Ngo-Duc, P. Singhruck, Ja. Santisirisomboon, W. Wongsaree, K. Promjirapawat, Y.  
687 Sukamongkol, R. Srisawadwong, D. Setsirichok, G. Narisma, S. T. Ngai, T. Phan-Van,  
688 E. Aldrian, D. Gunawan, G. Nikulin, & H. Yang (2019). Projected future changes in  
689 mean precipitation over Thailand based on multi-model regional climate simulations of  
690 CORDEX Southeast Asia. *International Journal of Climatology*, **39(14)**, 5413-  
691 5436, <https://doi.org/10.1002/joc.6163>
- 692 Tangang, F., S. Supari, J.X. Chung, F. Cruz, E. Salimun, S.T. Ngai, L. Juneng, Je.  
693 Santisirisomboon, Ja. Santisirisomboon, T. Ngo-Duc , T. Phan-Van, G. Narisma, P.  
694 Singhruck, D. Gunawan, E. Aldrian, A. Sopaheluwakan, G. Nikulin, H. Yang,  
695 A.R.C.Remedio, D. Sein, & D. Hein-Griggs (2018). Future changes in annual  
696 precipitation extremes over Southeast Asia under global warming of 2°C. *APN Science*  
697 *Bulletin*, **8(1)**, <https://doi.org/10.30852/sb.2018.436>
- 698 Tebaldi, C. and Knutti, R (2007). The Use of the Multi-Model Ensemble in  
699 Probabilistic Climate Change Projections, *Philosophical Transactions of The Royal*  
700 *Society A*, 365(1857):2053-75, <https://doi.org/10.1098/rsta.2007.2076>
- 701 Tibay, J, Cruz, F, Tangang, F, et al. Climatological characterization of tropical cyclones  
702 detected in the regional climate simulations over the CORDEX-SEA domain. *Int J*  
703 *Climatol.* 2021; 1–17. <https://doi.org/10.1002/joc.7070>

- 704 Trinh-Tuan, L., J. Matsumoto, F.T. Tangang, L. Juneng, F. Cruz, G. Narisma, J.  
705 Santisirisomboon, T. Phan-Van, D. Gunawan, E. Aldrian, & T. Ngo-Duc (2019)  
706 Application of Quantile Mapping Bias Correction for Mid-future Precipitation  
707 Projections over Vietnam. SOLA, 15, 1-6, <https://doi.org/10.2151/sola.2019-001>
- 708 Winterfeld, J., Geyer, B., Weisse, R. 2011. Using QuikSCAT in the added value  
709 assessment of dynamically downscaled wind speed. Int. J. Climatol. 31: 1028–1039.  
710 Doi:10.1002/joc.2105
- 711 Wu, L., Chou, C., Chen, C.-T., Huang, R., Knutson, T. R., Sirutis, J. J., Feng, Y.-C.  
712 (2014). Simulations of the Present and Late-Twenty-First-Century Western North  
713 Pacific Tropical Cyclone Activity Using a Regional Model. Journal of Climate, 27(9),  
714 3405–3424. <https://doi.org/10.1175/JCLI-D-12-00830.1>

# FIGURES AND TABLES

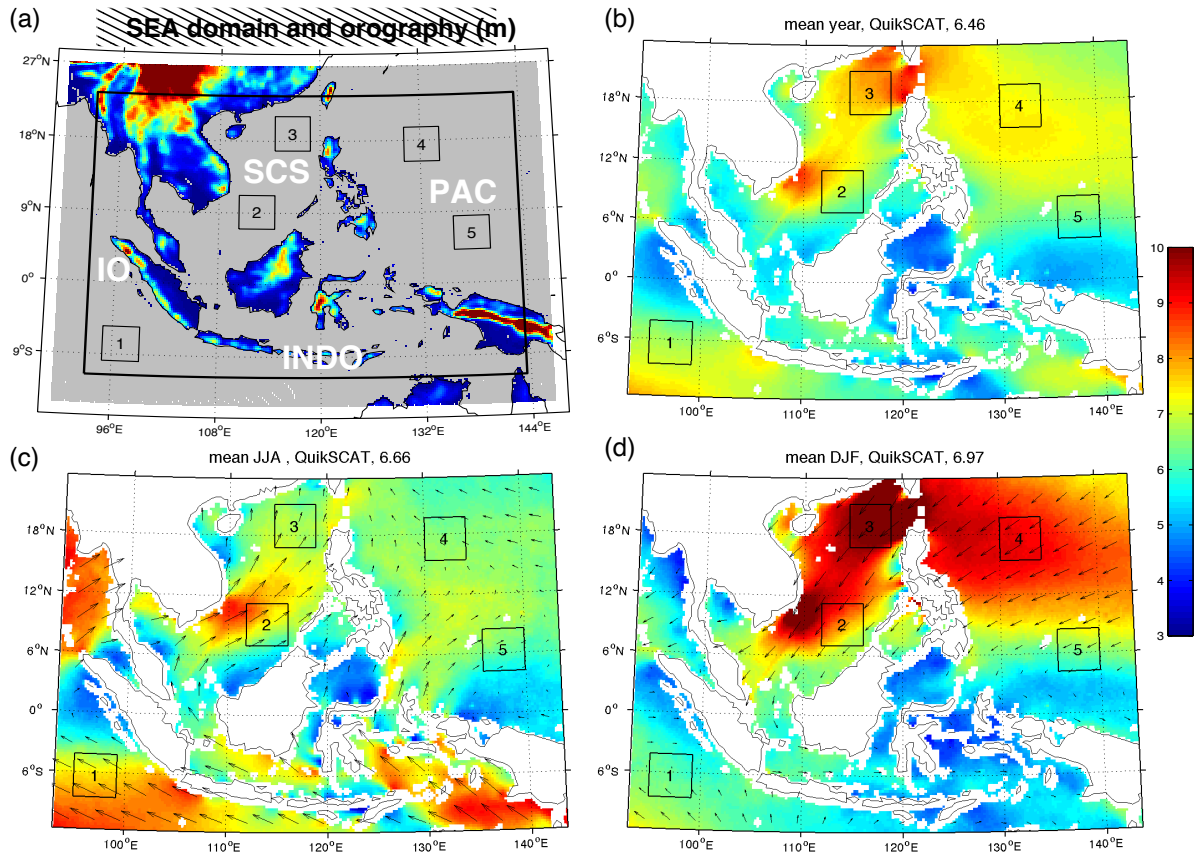
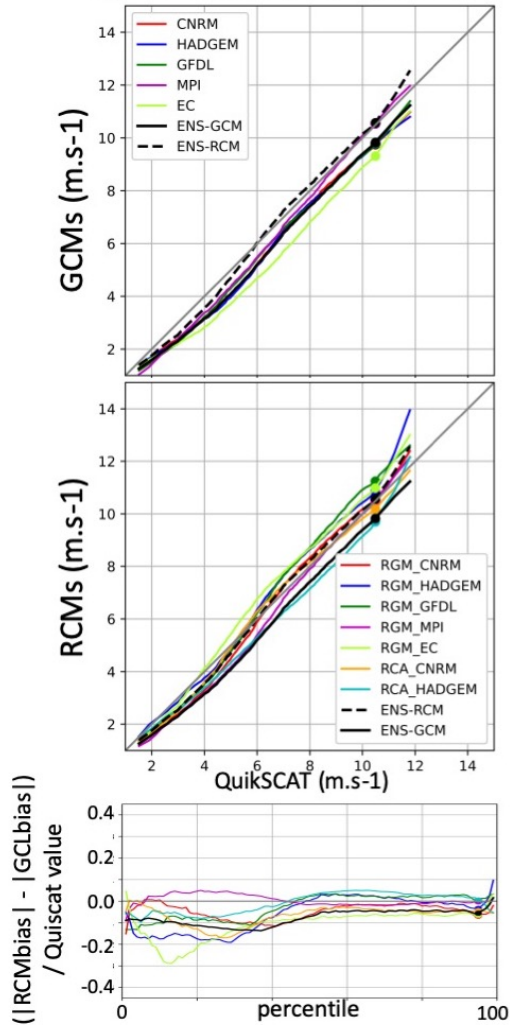
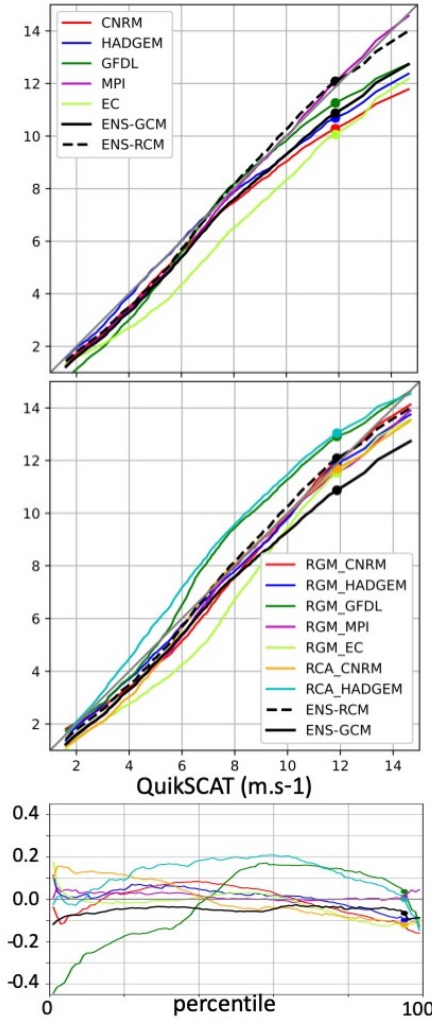


Figure 1 : (a) SEA domain (black frame) and orography (grey: sea; colors : land topography, m) and average over 2000-2008 of QuikSCAT daily winds over the b) the whole year, c) DJF and d) JJA (colors : wind speed, m; arrows : wind vector). Boxes B1-5 and main areas (IO, SCS, PAC, INDO) of the SEA domain are also indicated.

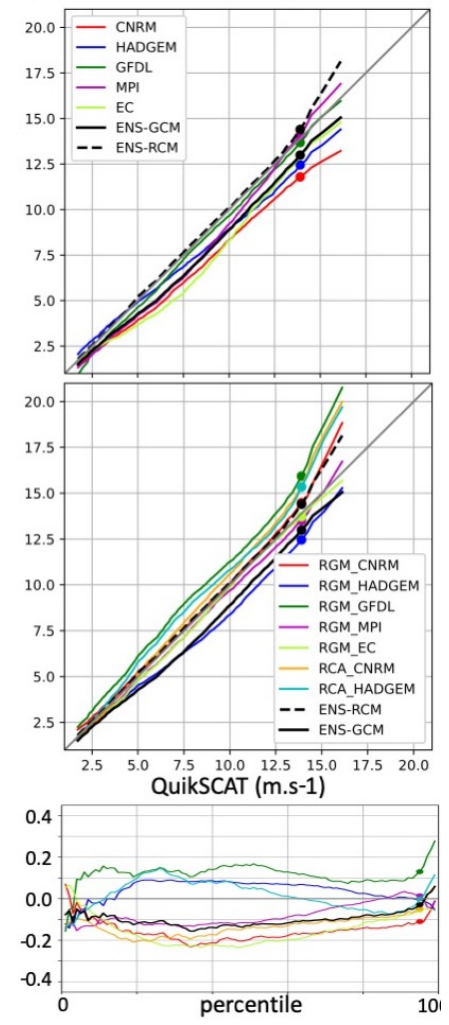
a) B1. Mean : 6.90 q95 : 10.49



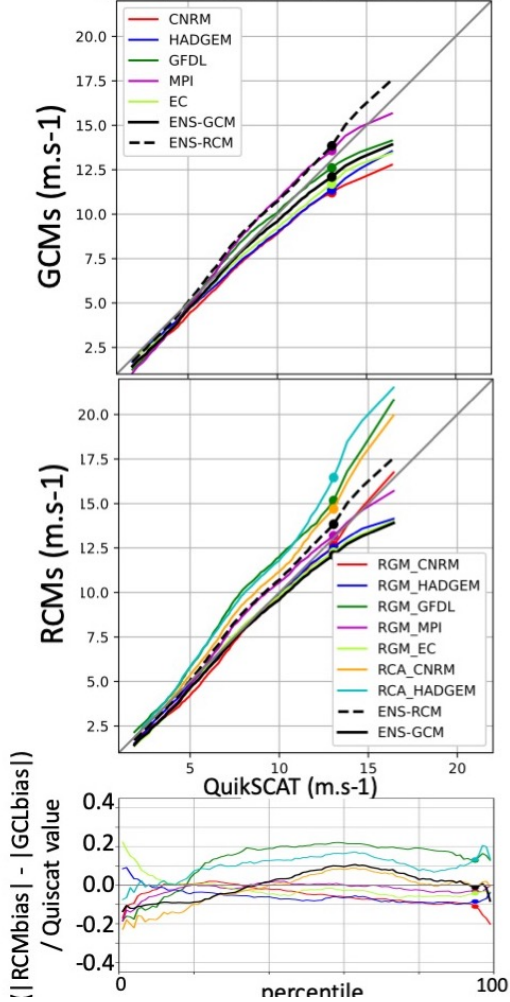
b) B2. Mean : 6.78 q95 : 11.87



c) B3. Mean : 7.85 q95 : 13.90



d) B4. Mean : 7.33 q95 : 13.05



e) B5. Mean : 6.26 q95 : 10.80

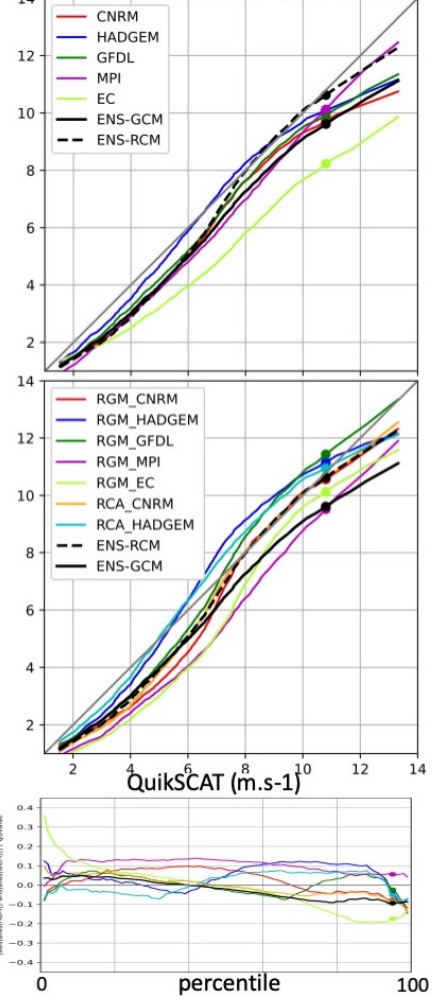


Figure 2: For boxes B1 (a) to B5 (e), each panel shows : the QQplots of sea surface wind speed ( $\text{m}\cdot\text{s}^{-1}$ ) averaged over the box for the period 2000-2008 for GCMs (top) and GCM\_RCMs (middle) runs vs. QuikSCAT ; (bottom) the difference of GCM and RCM bias relative to the QuikSCAT value for each percentile, for each RCM\_GCM pair and for the ensembles (black) : a negative value corresponds to an improvement in the downscaling. Dots : q95 values. QuikSCAT climatological average and q95 values are indicated in the title, and their relative biases for each GCM, GCM-RCM pair and for the ensembles are given in Table 3.

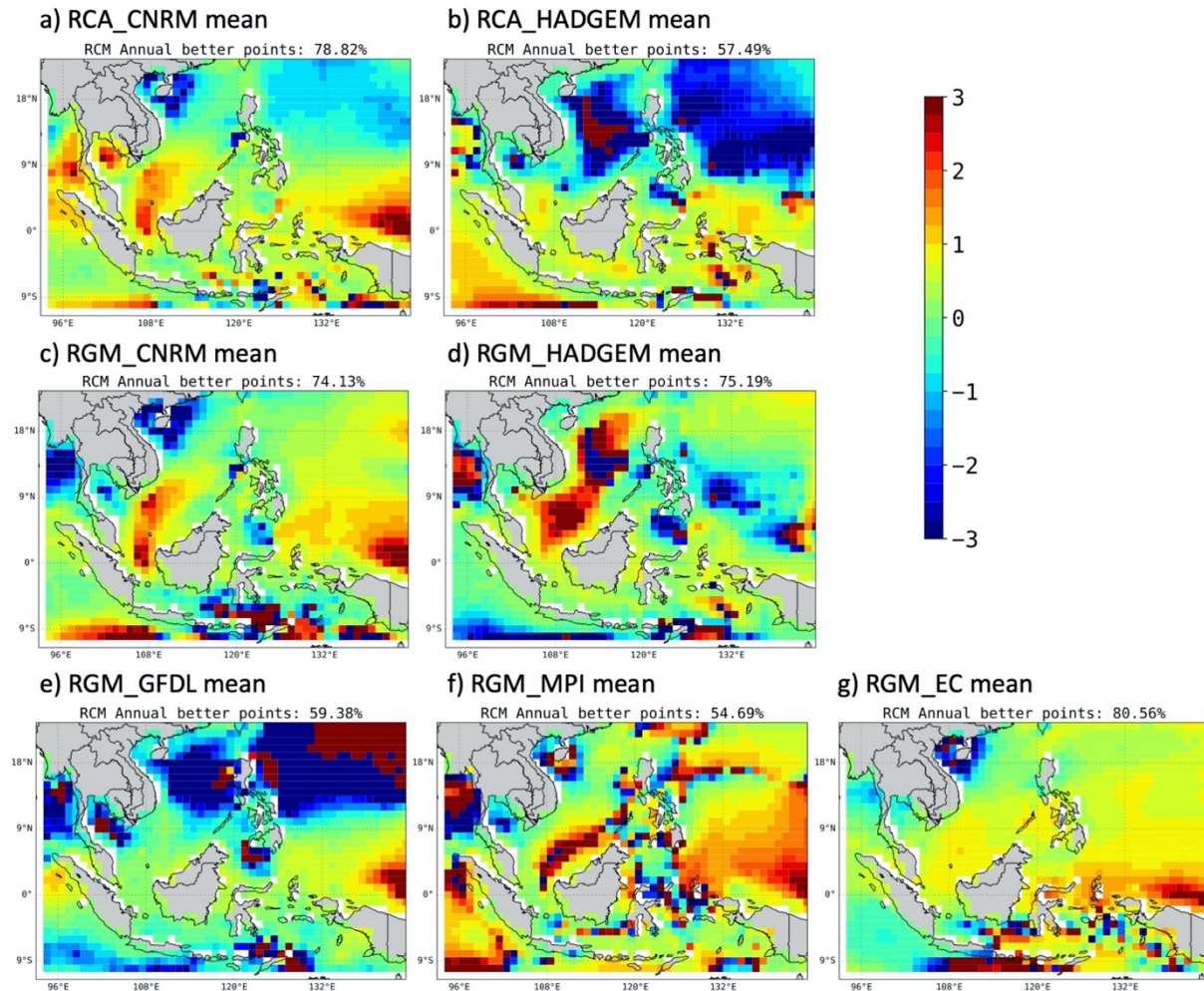


Figure 3 : RCM/GCMratio of the mean sea surface wind speed biases compared to QuikSCAT in each GCM\_RCM pair and corresponding GCM (a ratio between -1 and 1 corresponds to smaller bias in the RCM compared to the GCM). The percentage of SEA domain where the ratio is smaller than +/-1 is indicated in the title of each map.

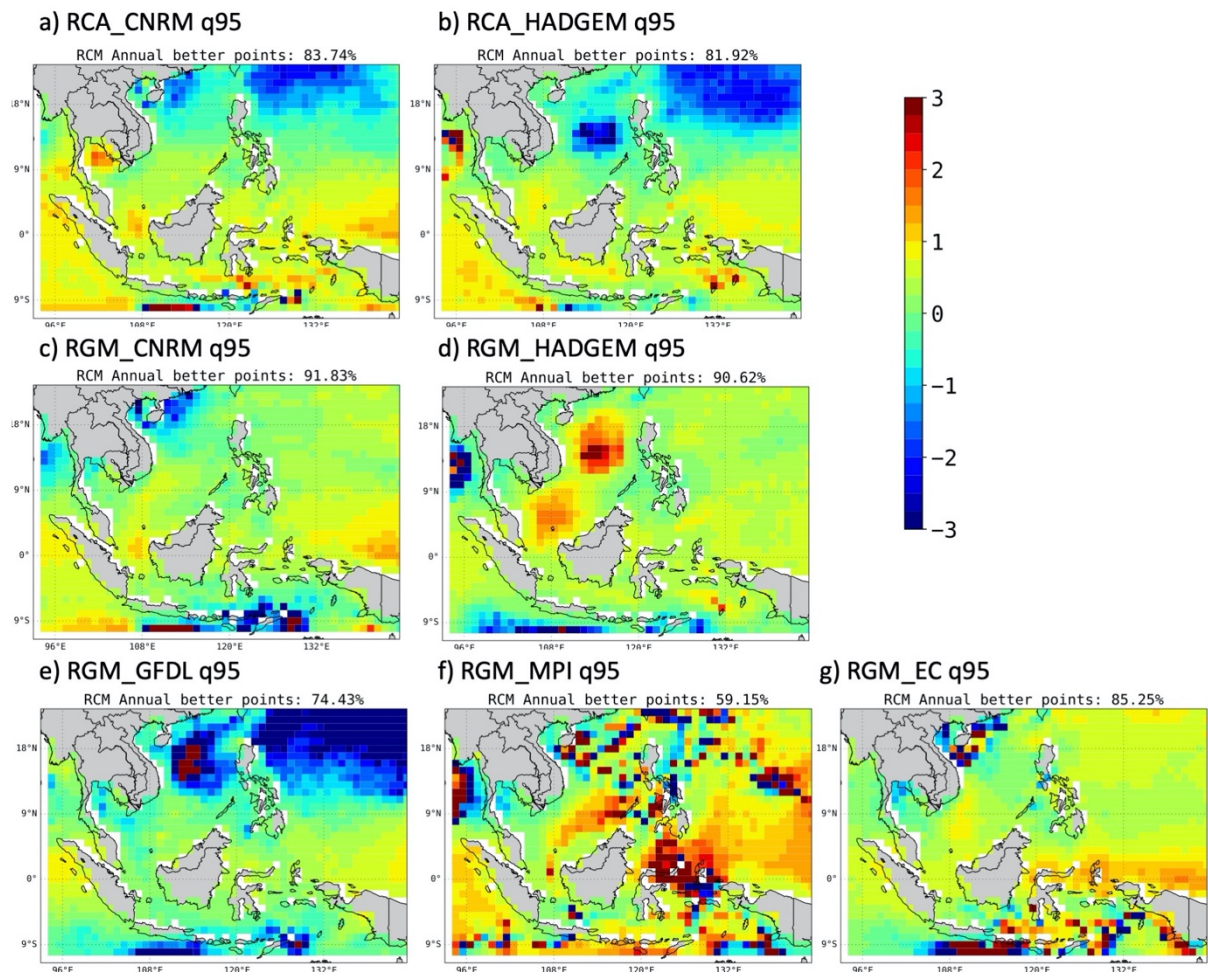


Figure 4 : Same as Figure 3 for q95.

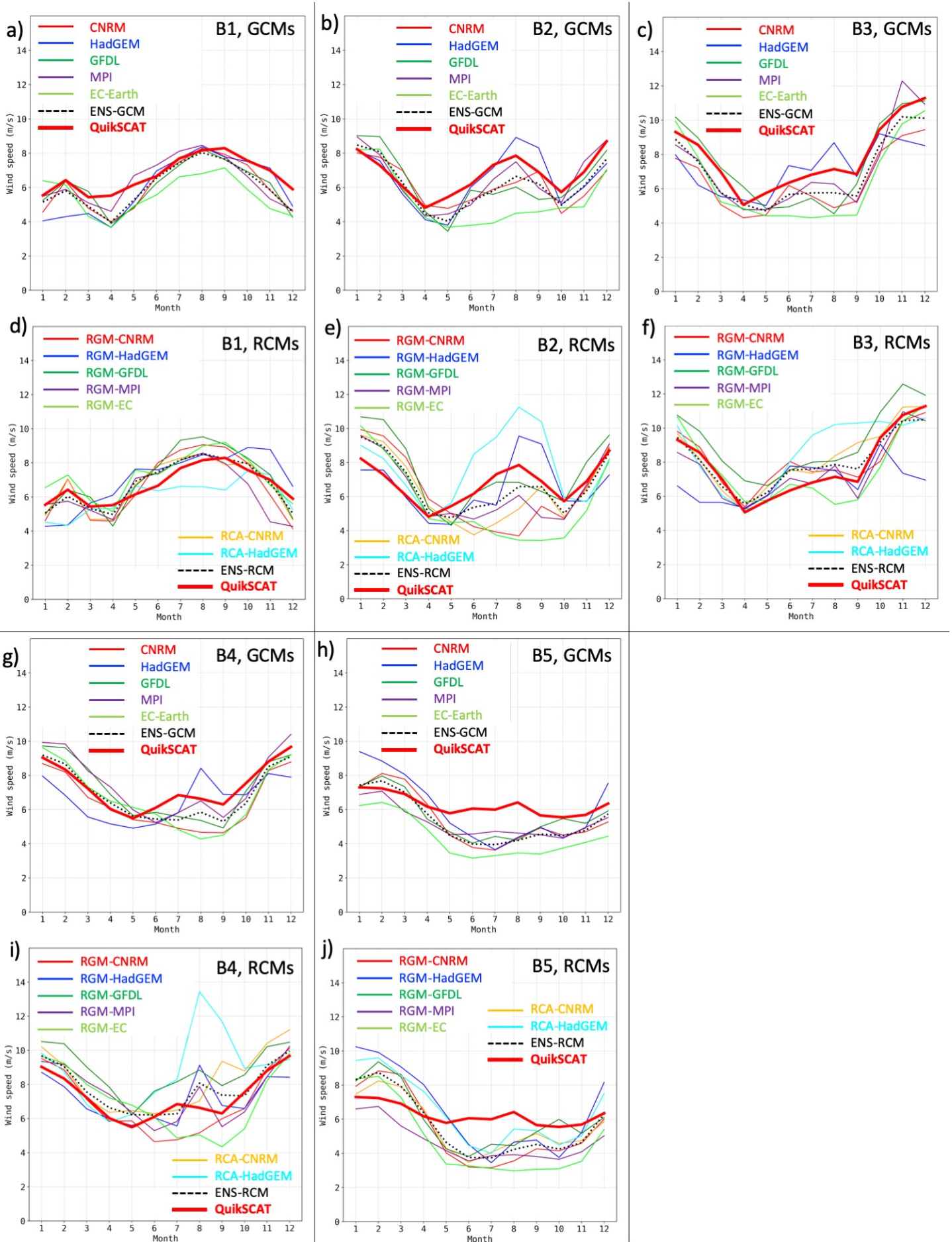


Figure 5. Climatological monthly time series of observed (QuikSCAT) and modeled sea surface wind speed ( $\text{m}\cdot\text{s}^{-1}$ ) averaged over boxes B1 to B5. Correlation coefficients between model and observations and associated p-value are given in Table 3 for each model and for the ENS-GCM and ENS-RCM ensembles.

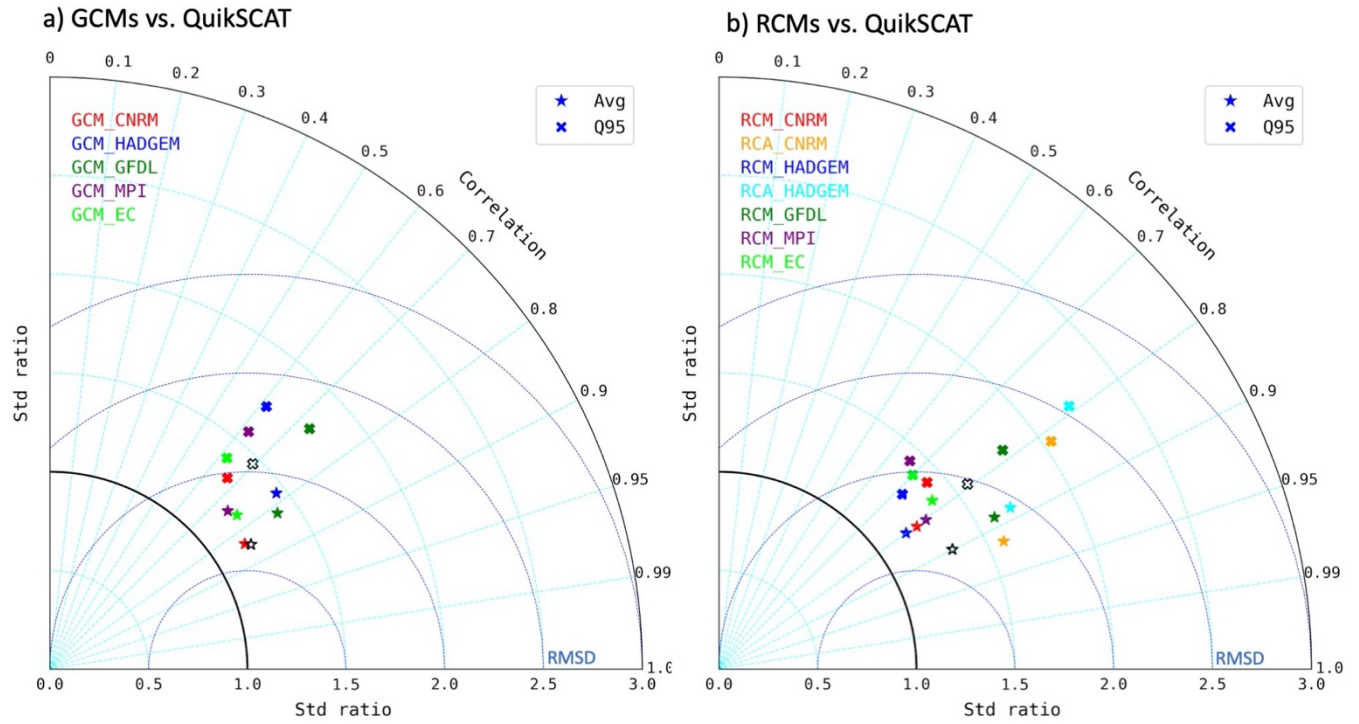


Fig. 6. Taylor diagram between models and QuikSCAT of the spatial fields over SEA of climatological mean (stars) and q95 (crosses) of daily sea surface wind speed over the period 2000-08. Black symbols correspond to ENS-GCM and ENS-RCM ensembles.

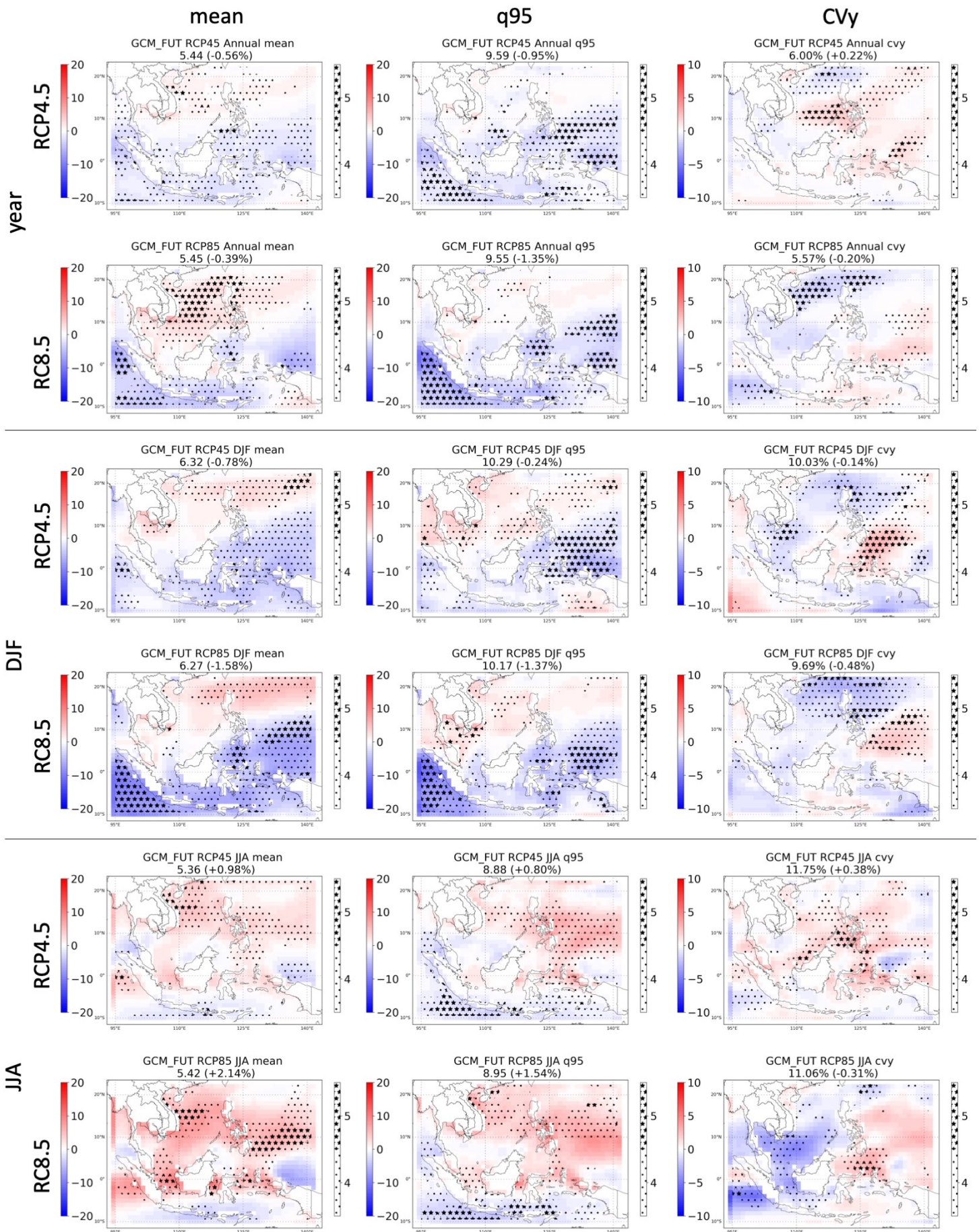


Figure 7. Maps of the relative variation (%) of the mean, CVy and q95 values of daily surface wind speed between HIST and FUT in RCP4.5 and RCP8.5 for ENS-GCM for the whole year, DJF and JJA. Mean SEA value and relative (%) differences between HIST and FUT are indicated in the titles. Large, resp. small stars indicate areas where all, i.e. 5, resp. 4 models produce a trend of the same sign.

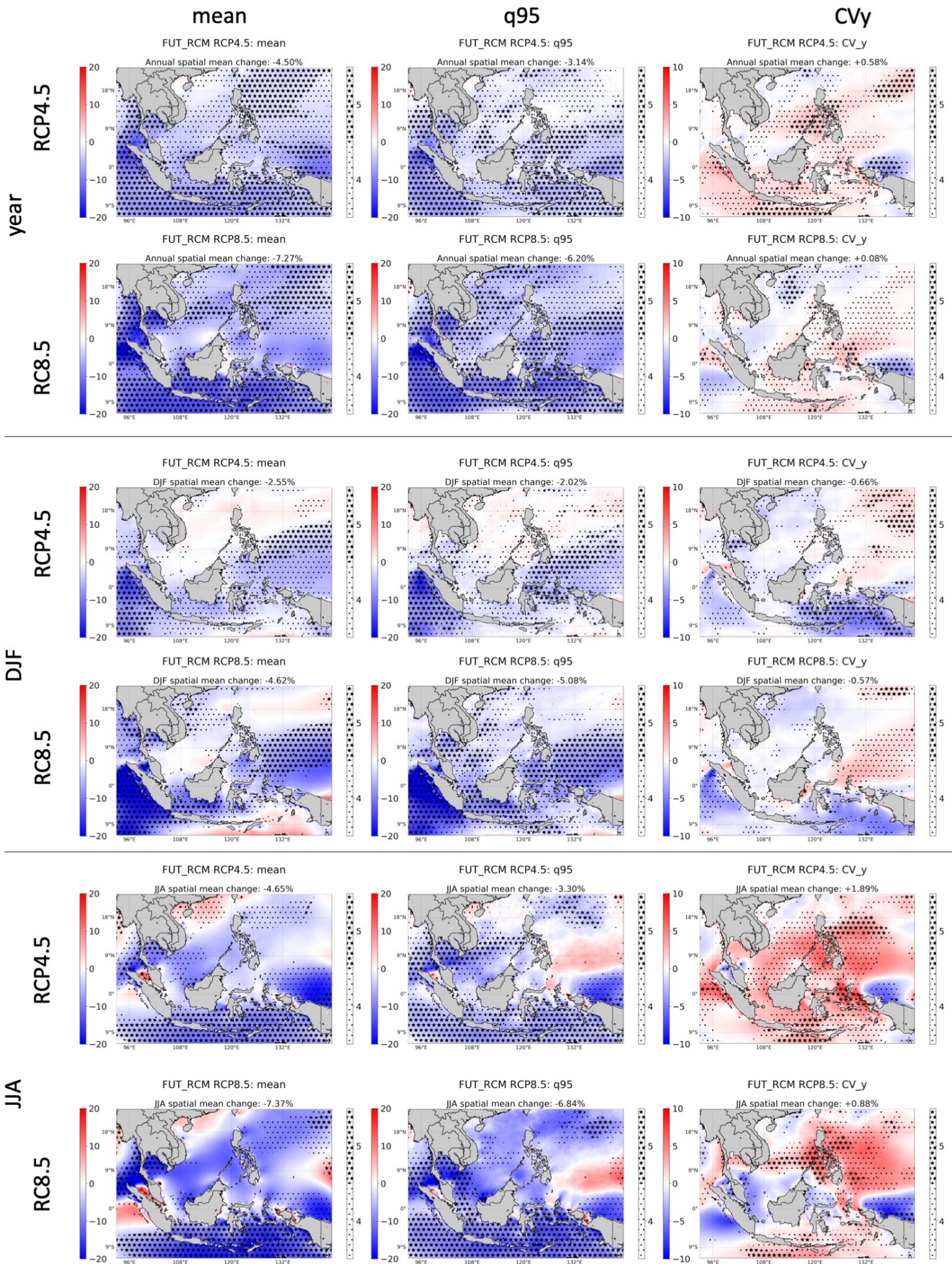


Figure 8. Same as Figure 7 for ENS-RGM.

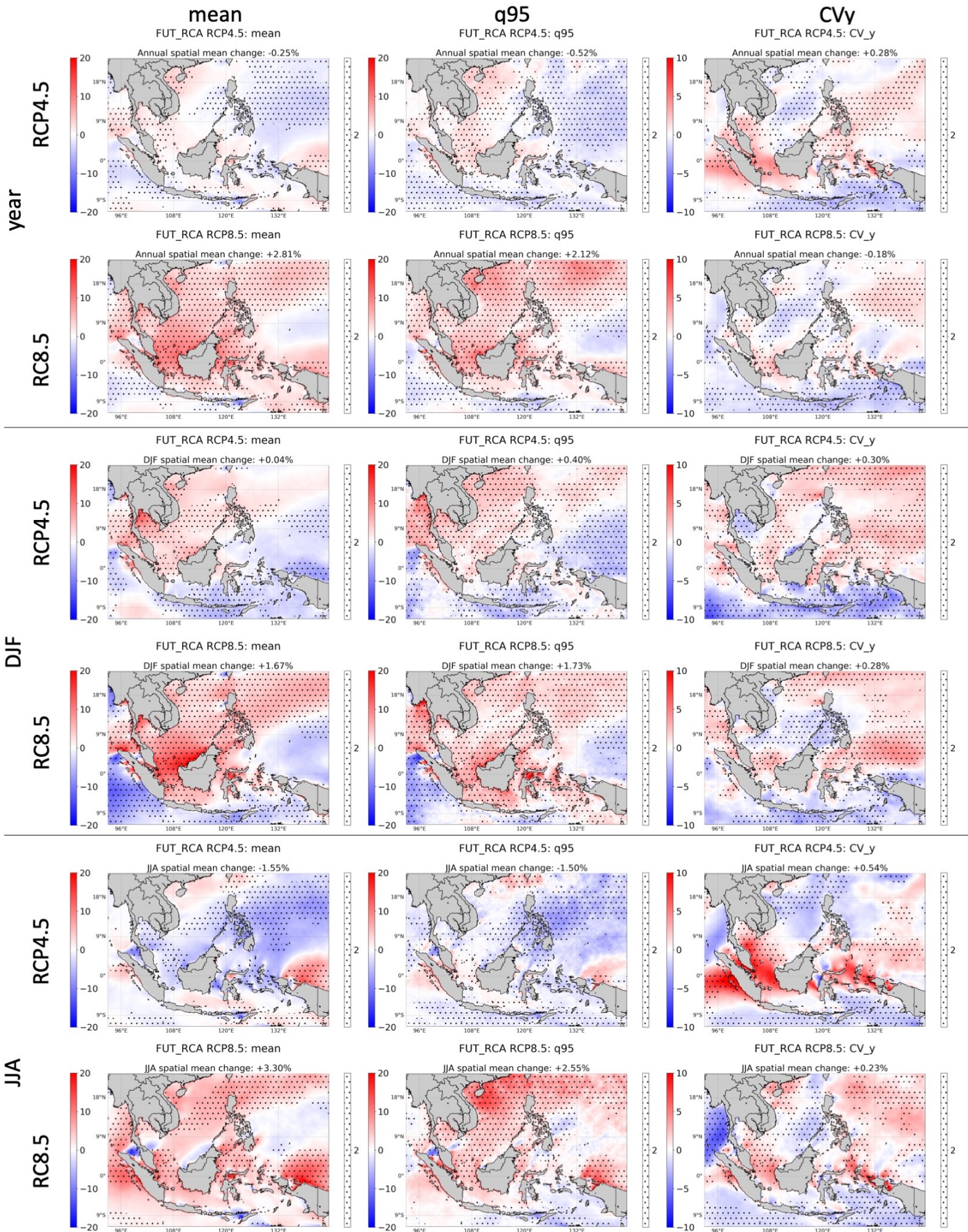
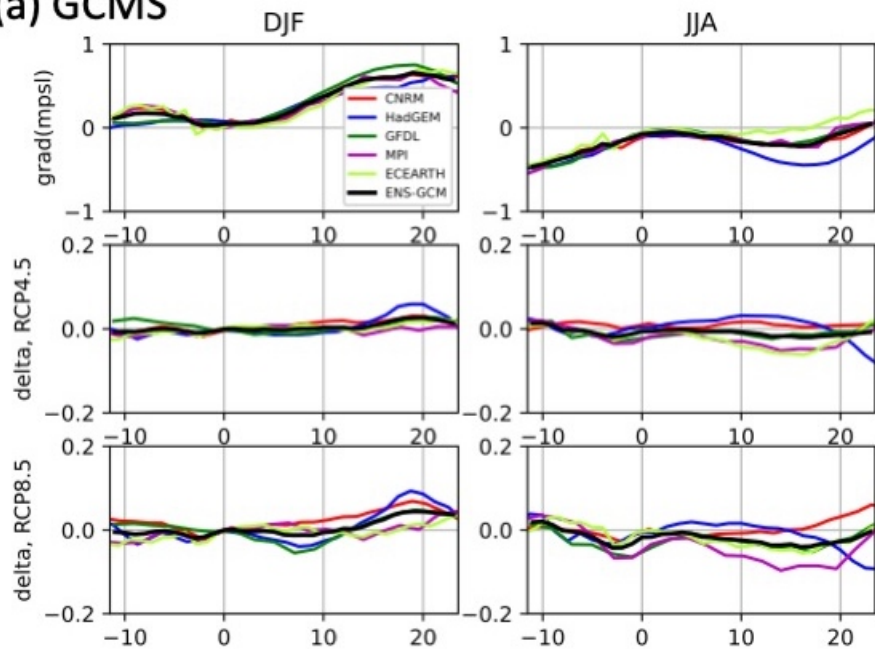
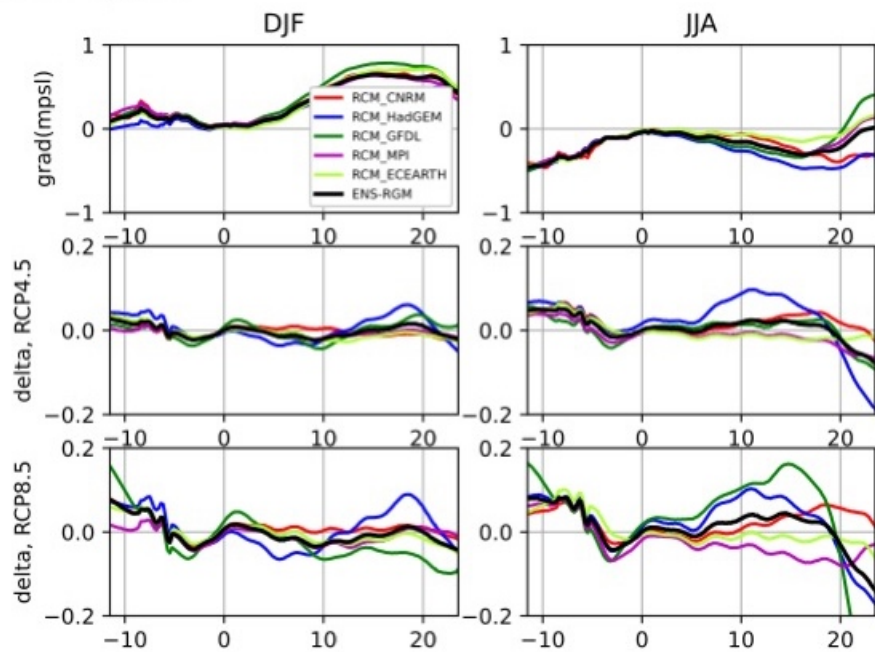


Figure 9. Same as Figure 7 for RCA. Small stars indicate areas where both2 RCA\_GCM runs produce a trend of the same sign.

### (a) GCMS



### (b) RegCM



### (c) RCA

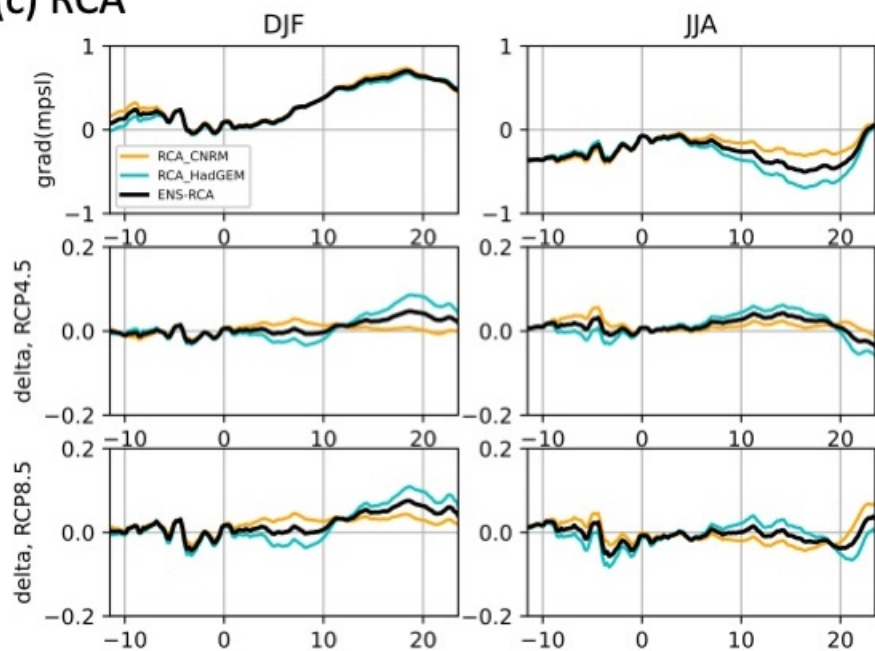


Figure 10. Each panel shows the meridional gradient (hPa/deg) of the mean sea level pressure over the HIST period (1<sup>st</sup> line) and changes between the HIST and FUT periods for RCP4.5 (2<sup>nd</sup> line) and RCP8.5 (3<sup>rd</sup> line), for DJF (left) and JJA (right), for each GCM (a), RegCM (b) and RCA (c) run and for their ensembles.

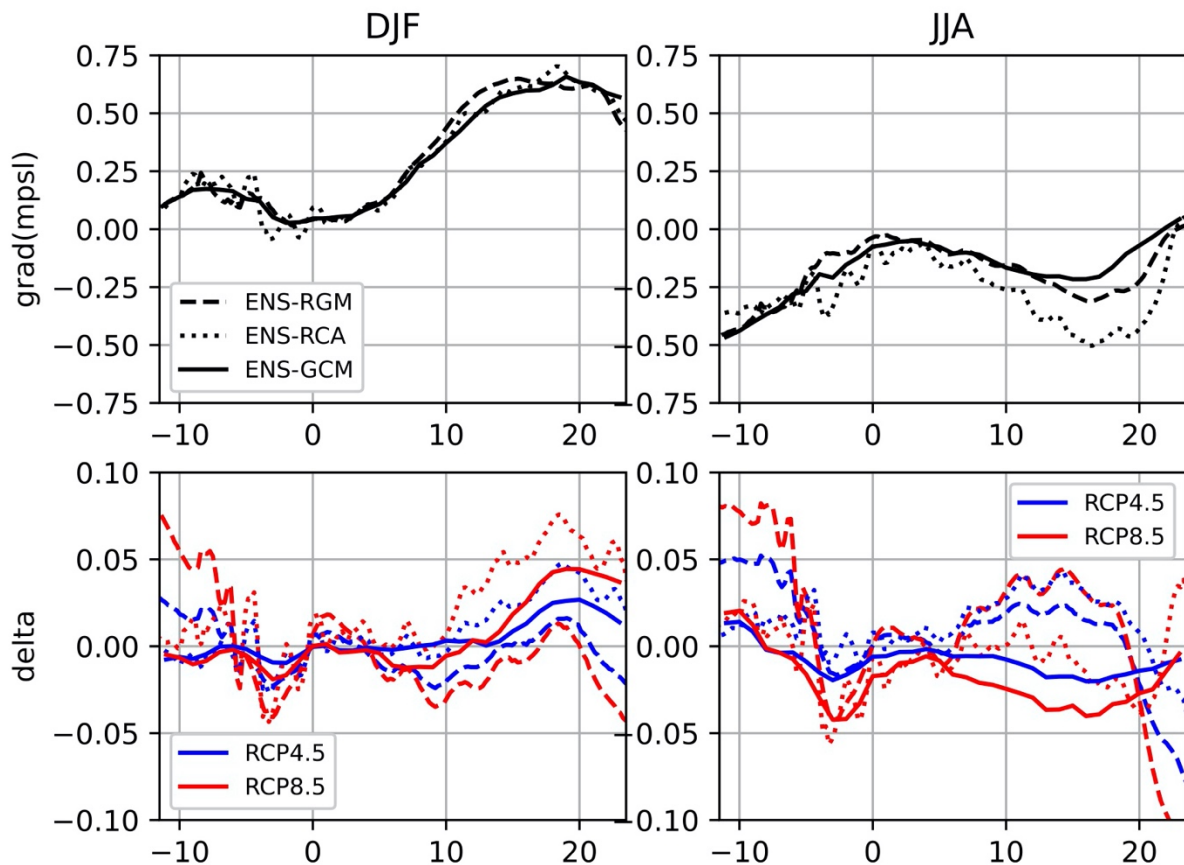


Figure 11. Meridional gradient (hPa/deg) of the mean sea level pressure over the HIST period (top) and changes between the HIST and FUT periods (bottom) for RCP4.5 (blue) and RCP8.5 (red), for DJF (left) and JJA (right) for the 3 ENS-GCM (full line), ENS-RCA (dotted line) and ENS-RGM (dashed line) ensembles.

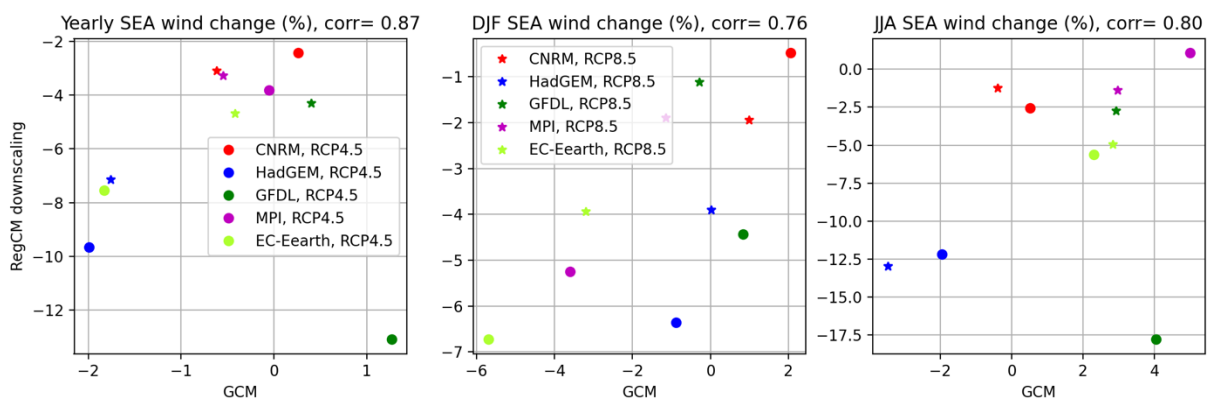


Figure 12. SEA average relative changes (from Table 4) for each GCM vs. the corresponding RegCM downscaling for the yearly, DJF and JJA averages. “Corr” indicates the correlation coefficient (all with p-values smaller than or equal to 0.01) between the GCM and RCM values excluding RGM\_HadGEM value for RCP8.5 (green dot).

Table 1. Overview of CMIP5 GCM runs and RCM\_GCM downscaled runs. Near-surface monthly and daily wind RCMs and GCMs outputs are available on ESGF cores (<https://esgf.llnl.gov/>) and on USTH server ([http://remosat.usth.edu.vn//Download/dat\\_was\\_CORDEX](http://remosat.usth.edu.vn//Download/dat_was_CORDEX)).

RCM_GCM pair	RCM (see Tangang et al. 2019, 2020 for details)	GCM and reference	Group
RGM_CNRM	RegCM4	CNRM-CM5 (Centre National de Recherches Météorologiques, France), Voldoire et al. (2013)	University of Sciences and Technology of Hanoi, USTH, Vietnam
RGM_HADGEM	RegCM4	HadGEM2 (Hadley Centre, UK), Martin et al., (2011)	Ateneo de Manila University and Manila Observatory, AMU, Philippines
RGM_GFDL	RegCM4	GFDL (Geophysical Fluid Dynamics Laboratory, USA), Dunne et al. (2012, 2013)	National University of Malaysia, UKM, Malaysia
RGM_MPI	RegCM4	MPI-ESM-MR (Max-Planck-Institut für Meteorologie, Germany), Jungclaus et al. (2010)	Ramkhamhaeng University Center of Regional climate change and Renewable Energy, RU-CORE, Thailand
RGM_EC	RegCM4	EC-Earth (EC-Earth Consortium, European Community), Hazeleger et al. (2012)	Ramkhamhaeng University Center of Regional climate change and Renewable Energy, RU-CORE, Thailand
RCA_CNRM	RCA4	CNRM-CM5, Voldoire et al. (2013)	Swedish Meteorological and Hydrological Institute, SMHI, Sweden
RCA_HADGEM	RCA4	HadGEM2, Martin et al. (2011)	Swedish Meteorological and Hydrological Institute, SMHI, Sweden

Table 2 : Relative mean and q95 biases (%) of sea surface wind speed compared to QuikSCAT over 2000-2008 in average over boxes B1 to B5 and over the SEA for the 5 GCMs and the 7 RCM\_GCM pairs. Color code : black : absolute value of bias > 20%; red : > 15%; orange : >10%; cyan : > 5%; blue : < 5%

ENS-GCM		B1	B2	B3	B4	B5	SEA	ENS-RCM		B1	B2	B3	B4	B5	SEA
CNRM	mean	-9,6	-9,4	-18,0	-12,5	-13,5	-17,1	RGM_CNRM	mean	-0,5	-6,7	3,1	-5,3	-13,9	-3,7
	q95	-7,2	-13,4	-15,2	-14,1	-10,0	-21,0		q95	0,2	1,0	4,1	-3,1	-2,2	-6,0
								RCA_CNRM							
HadGEM	mean	-10,3	-4,0	-8,1	-9,6	-3,5	-18,4	RGM_HadGEM	mean	5,5	-3,5	-12,9	-2,6	3,7	-1,4
	q95	-7,0	-10,0	-10,4	-12,9	-6,6	-26,5		q95	3,6	0,0	-10,3	-4,5	3,2	-8,3
								RCA_HadGEM							
GFDL	mean	-9,1	-6,9	-4,1	-1,2	-10,9	-15,3	RGM_GFDL	mean	5,0	9,3	16,4	20,2	-4,8	8,1
	q95	-6,8	-5,1	-1,6	-3,5	-8,2	-20,9		q95	7,1	8,8	14,6	16,2	5,8	2,7
MPI	mean	-5,4	-4,6	-8,9	2,7	-16,3	-6,3	RGM_MPI	mean	-5,5	-6,0	-3,4	2,3	-25,7	-3,9
	q95	0,4	1,5	1,3	4,0	-6,3	-8,3		q95	-0,1	-2,6	-2,8	1,0	-11,9	-4,7
EC-Earth	mean	-17,2	-21,8	-17,6	-7,9	-30,1	-17,5	RGM_EC	mean	7,6	-17,6	-2,8	-4,0	-24,5	-7,3
	q95	-11,3	-15,2	-6,8	-10,4	-23,8	-19,1		q95	4,7	-2,8	-1,3	-6,1	-6,3	-8,5
ENS-GCM	mean	-10,3	-9,3	-11,3	-5,7	-14,9	-15,1	ENS-RCM	mean	0,3	-2,2	2,5	6,2	-10,4	-1,1
	q95	-6,4	-8,4	-6,5	-7,4	-11,0	-19,1		q95	0,7	1,8	3,6	6,0	-1,6	-4,4

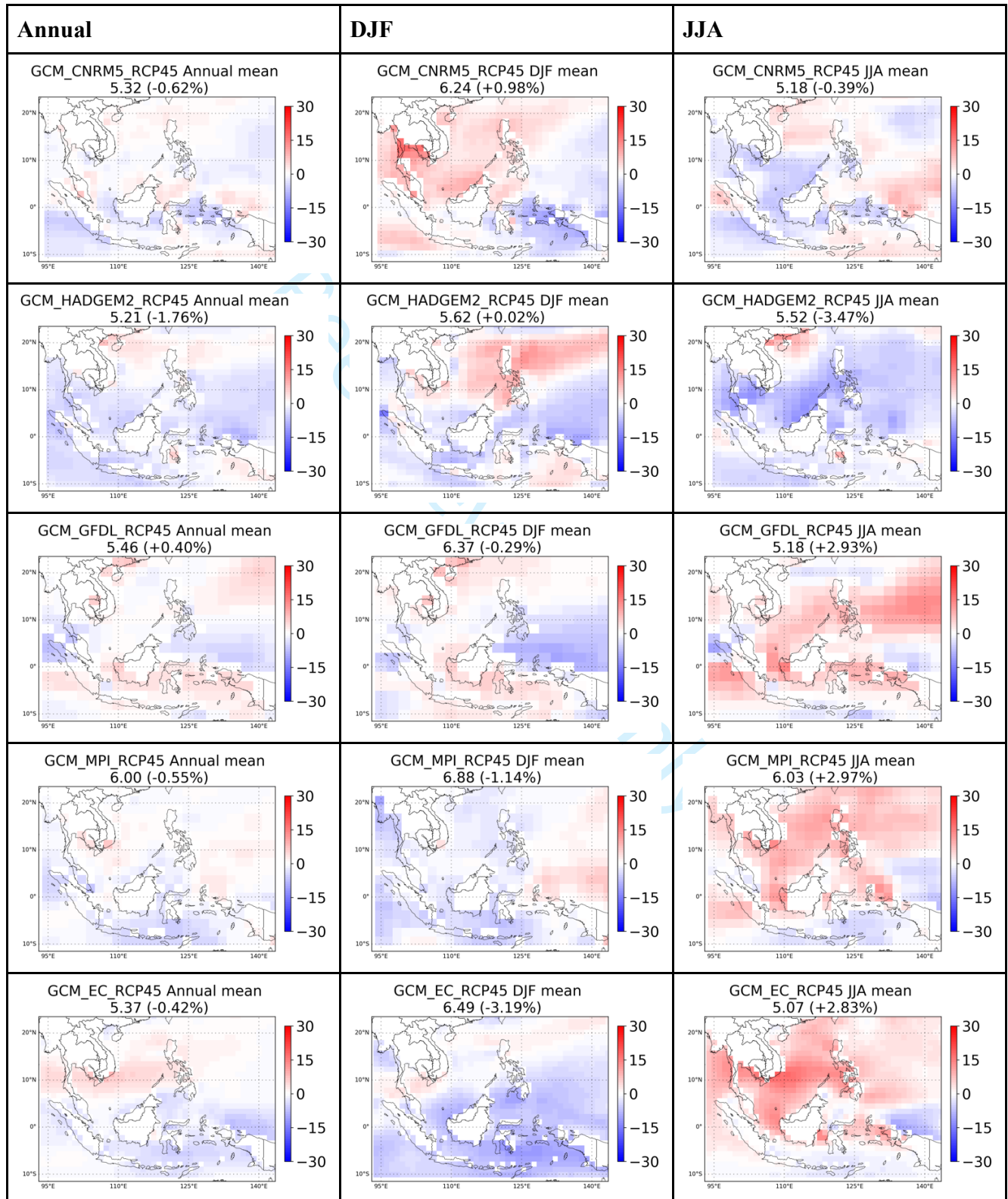
Table 3 : correlation coefficient between monthly climatological time series of sea surface wind in QuikSCAT and in GCM and RCM runs. Color code : blue > 0.90; light blue > 0.80; black > 0.71 (corresponding to p-value >0.01); red < 0.71

GCM	B1	B2	B3	B4	B5	RCM_GCM	B1	B2	B3	B4	B5
CNRM	0,95	0,72	0,96	0,88	0,81	RGM_CNRM	0,92	0,4	0,92	0,91	0,82
						RCA_CNRM	0,90	0,59	0,91	0,87	0,82
HADGEM	0,93	0,86	0,74	0,71	0,85	RGM_HADGEM	0,74	0,70	0,37	0,71	0,84
						RCA_HADGEM	0,67	0,69	0,69	0,25	0,86
GFDL	0,89	0,72	0,91	0,86	0,78	RGM_GFDL	0,93	0,72	0,98	0,94	0,79
MPI	0,84	0,94	0,95	0,89	0,92	RGM_MPI	0,76	0,71	0,94	0,82	0,91
EC-EARTH	0,73	0,59	0,92	0,81	0,86	RGM_EC	0,90	0,47	0,91	0,73	0,91
ENS-GCM	0,95	0,86	0,98	0,92	0,86	ENS-RCM	0,94	0,76	0,96	0,92	0,87

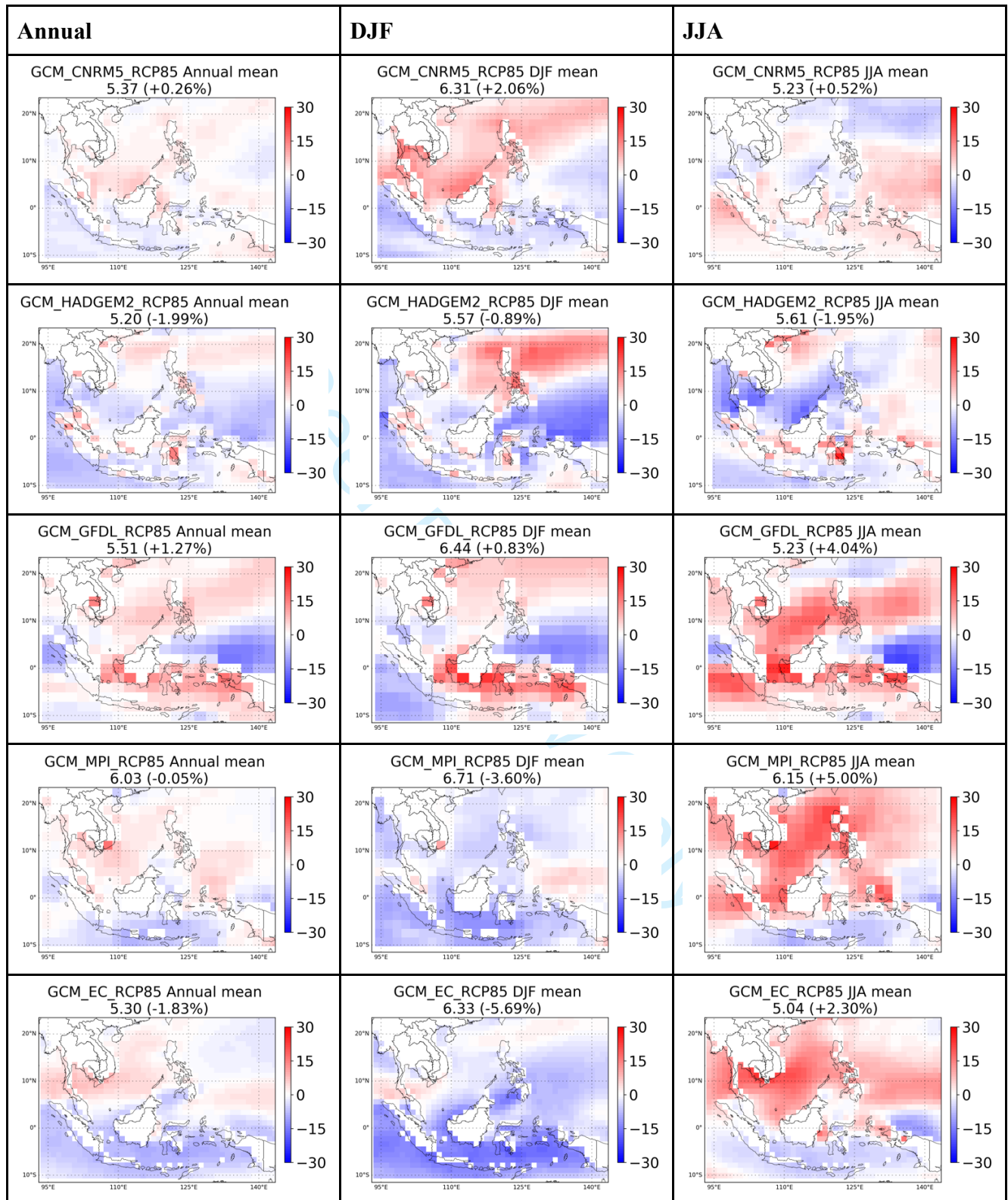
Table 4 : relative changes (%) on SEA average of seasonal average, q95 and CVy of daily sea surface wind speed for the whole year, DJF and JJA in all GCMs and RCMs runs, and in ENS-GCM, ENS-RGM and ENS-RCA ensembles. Color code : black : <-10%; blue <-5%; light blue <-1%; green <0%; orange >0%; magenta >1%; red >5%. Changes stronger that +/- 1 % are highlighted in grey cells.

GCMs			year	DJF	JJA	RegCM4			Year	DJF	JJA	RCA4			Year	DJF	JJA
CNRM	mean	rcp4,5	-0,62	0,98	-0,39	RGM_CNRM	mean	rcp4,5	-3,10	-1,94	-1,23	RCA_CNRM	mean	rcp4,5	-0,12	0,35	-1,14
		rcp8,5	0,26	2,06	0,52			rcp8,5	-2,43	-0,48	-2,54			rcp8,5	3,10	2,64	2,51
	q95	rcp4,5	-0,21	1,34	0,01		q95	rcp4,5	-2,41	-1,56	1,39		q95	rcp4,5	-0,42	0,52	-1,48
		rcp8,5	0,48	1,67	0,78		rcp8,5	-2,03	-0,81	-0,04	rcp8,5		1,86	2,21	2,23		
	CVy	rcp4,5	1,14	0,36	1,84		CVy	rcp4,5	0,91	0,32	4,25		CVy	rcp4,5	0,93	1,06	1,34
		rcp8,5	0,28	0,00	0,54		rcp8,5	-0,39	-0,02	4,11	rcp8,5		-0,36	0,51	0,97		
HadGEM	mean	rcp4,5	-1,76	0,02	-3,47	RGM_HadGEM	mean	rcp4,5	-7,14	-3,90	-12,96	RCA_HadGEM	mean	rcp4,5	-0,38	-0,18	-1,99
		rcp8,5	-1,99	-0,89	-1,95			rcp8,5	-9,66	-6,36	-12,18			rcp8,5	2,57	0,84	4,14
	q95	rcp4,5	-2,26	0,27	-4,70		q95	rcp4,5	-5,27	-3,19	-9,41		q95	rcp4,5	-0,61	0,41	-1,52
		rcp8,5	-2,73	-0,96	-3,02		rcp8,5	-7,58	-6,07	-8,11	rcp8,5		2,53	1,38	3,02		
	CVy	rcp4,5	-0,32	0,14	-0,42		CVy	rcp4,5	0,81	-1,02	1,79		CVy	rcp4,5	-0,36	-0,39	-0,28
		rcp8,5	-0,14	0,18	0,17		rcp8,5	0,66	-0,65	-0,04	rcp8,5		0,02	0,10	-0,47		
GFDL	mean	rcp4,5	0,40	-0,29	2,93	RGM_GFDL	mean	rcp4,5	-4,30	-1,11	-2,75						
		rcp8,5	1,27	0,83	4,04			rcp8,5	-13,09	-4,43	-17,81						
	q95	rcp4,5	0,36	0,68	1,66		q95	rcp4,5	-2,11	-0,80	-2,17						
		rcp8,5	-0,55	0,88	-0,05		rcp8,5	-12,61	-9,80	-22,65							
	CVy	rcp4,5	-0,84	-1,35	0,17		CVy	rcp4,5	1,00	-1,20	3,65						
		rcp8,5	-3,64	-2,88	-4,23		rcp8,5	-2,18	-3,56	-1,03							
MPI	mean	rcp4,5	-0,55	-1,14	2,97	RGM_MPI	mean	rcp4,5	-3,28	-1,89	-1,37						
		rcp8,5	-0,05	-3,60	5,00			rcp8,5	-3,82	-5,25	1,08						
	q95	rcp4,5	-1,32	-1,49	2,50		q95	rcp4,5	-2,77	-1,78	-1,40						
		rcp8,5	-1,39	-3,77	3,73		rcp8,5	-3,84	-4,75	-0,60							
	CVy	rcp4,5	0,05	-1,09	0,56		CVy	rcp4,5	0,65	-1,61	2,54						
		rcp8,5	-0,27	-0,70	-0,56		rcp8,5	0,97	-0,91	0,80							
EC-EARTH	mean	rcp4,5	-0,42	-3,19	2,83	RGM_EC	mean	rcp4,5	-4,68	-3,94	-4,96						
		rcp8,5	-1,83	-5,69	2,30			rcp8,5	-7,54	-6,73	-5,64						
	q95	rcp4,5	-0,61	-1,73	4,79		q95	rcp4,5	-3,19	-2,74	-4,97						
		rcp8,5	-1,22	-4,11	6,19		rcp8,5	-5,03	-4,03	-2,99							
	CVy	rcp4,5	0,37	1,22	-0,27		CVy	rcp4,5	-0,45	0,20	-2,73						
		rcp8,5	1,99	0,95	2,57		rcp8,5	1,33	2,29	0,61							
ENS-GCM	mean	rcp4,5	-0,56	-0,78	0,98	ENS-RGM	mean	rcp4,5	-4,50	-2,60	-4,70	ENS-RCA	mean	rcp4,5	-0,30	0,00	-1,50
		rcp8,5	-0,39	-1,58	2,14			rcp8,5	-7,30	-4,60	-7,40			rcp8,5	2,80	1,70	3,30
	q95	rcp4,5	-0,95	-0,24	0,80		q95	rcp4,5	-3,10	-2,00	-3,30		q95	rcp4,5	-0,50	0,40	-1,50
		rcp8,5	-1,35	-1,37	1,54		rcp8,5	-6,20	-5,10	-6,90	rcp8,5		2,10	1,70	2,60		
	CVy	rcp4,5	0,22	-0,14	0,38		CVy	rcp4,5	0,58	-0,66	1,89		CVy	rcp4,5	0,28	0,30	0,54
		rcp8,5	-0,20	-0,48	-0,31		rcp8,5	0,08	-0,57	0,88	rcp8,5		-0,18	0,28	0,23		

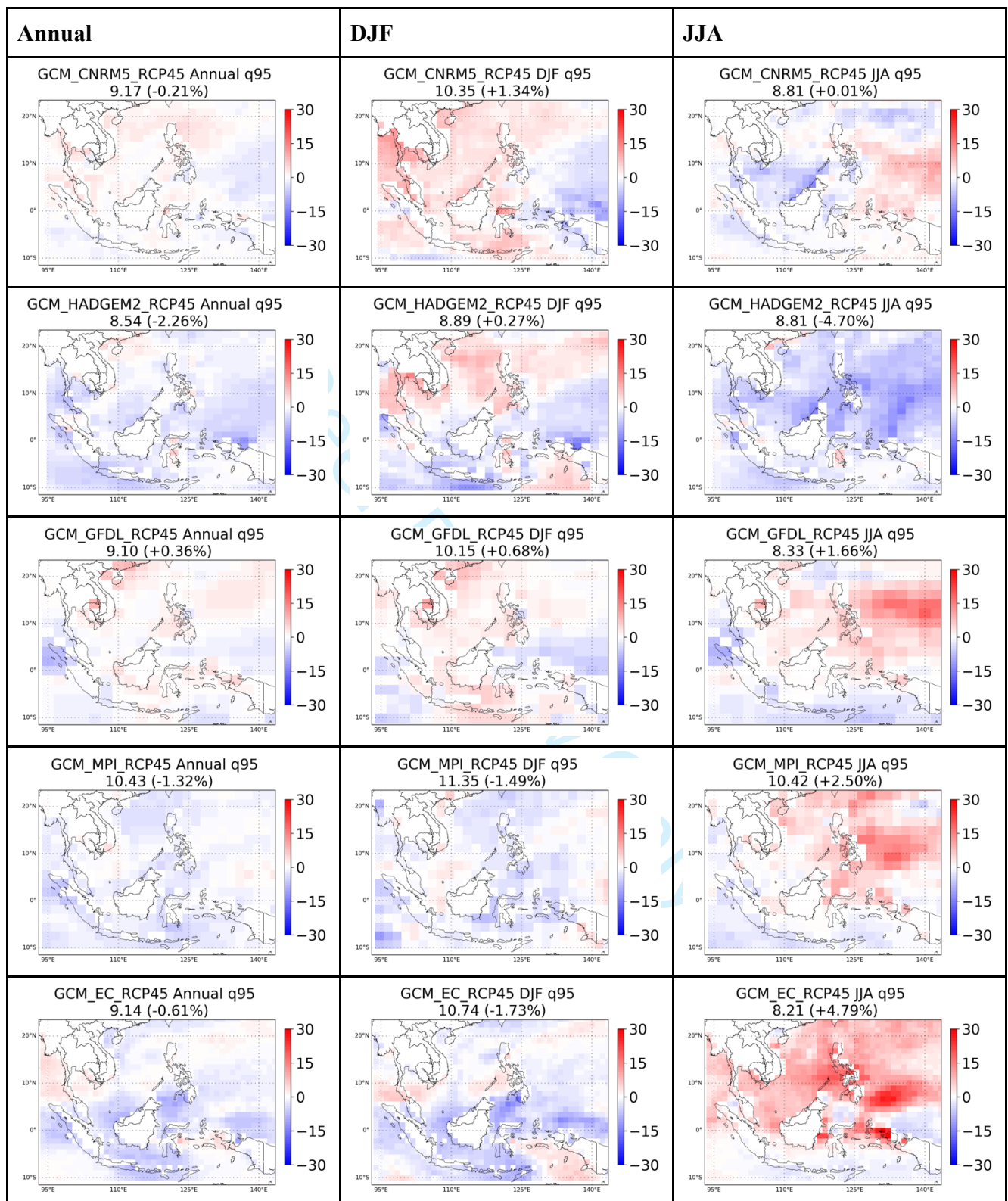
**Figure SM1. Maps of the relative change (%) between the HIST and FUT periods of the average wind (m.s-1) for the whole year (left), DJF (middle) and JJA (right) for each of the 5 GCMs in RCP4.5. Average value of average wind over the SEA and its relative variation between HIST and FUT are indicated in the titles.**



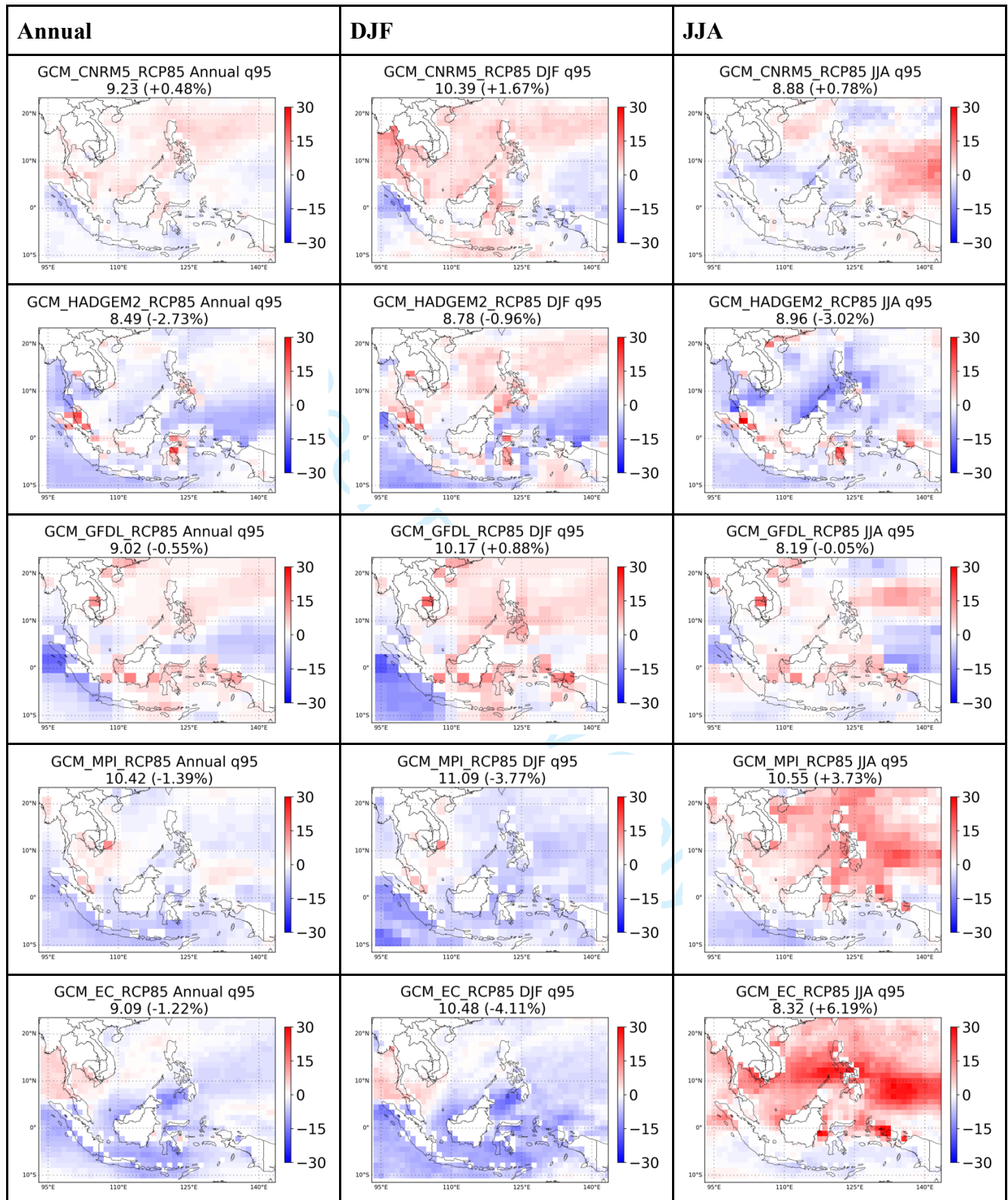
**Figure SM2. Same as Figure SM1 for RCP8.5.**



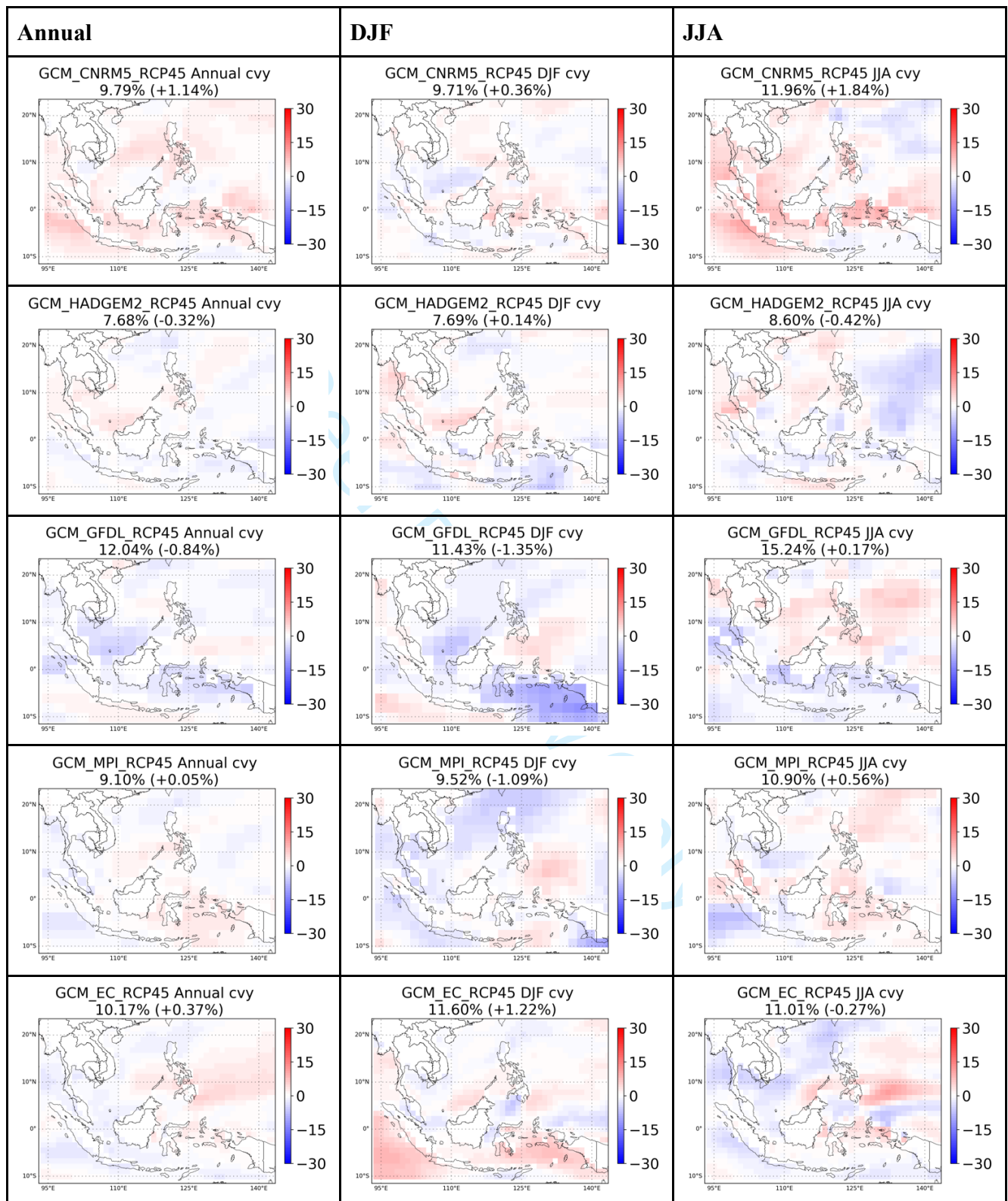
**Figure SM3. Same as Fig. SM1 for q95 (m.s-1).**



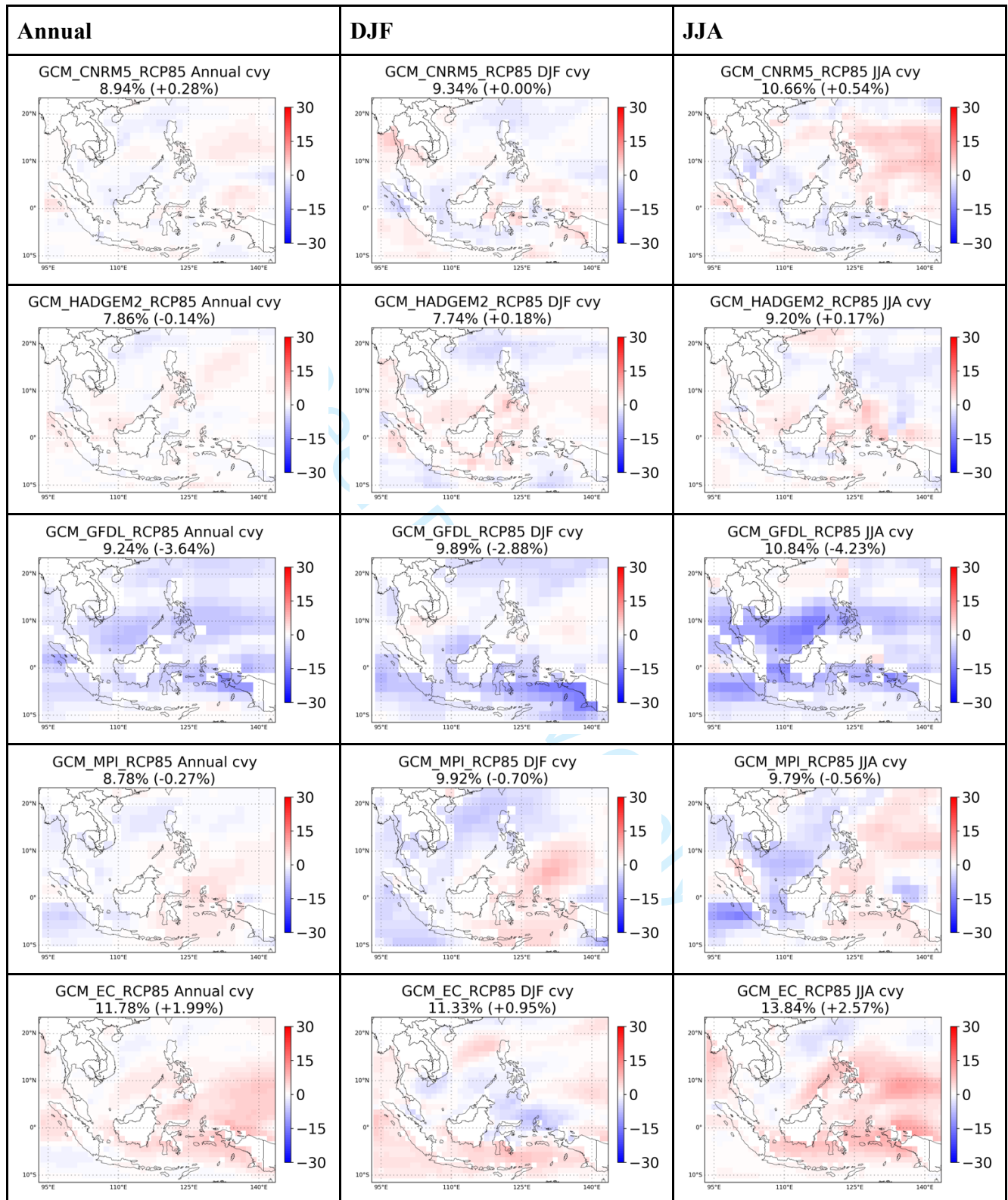
**Figure SM4. Same as Fig. SM3 for RCP8.5.**



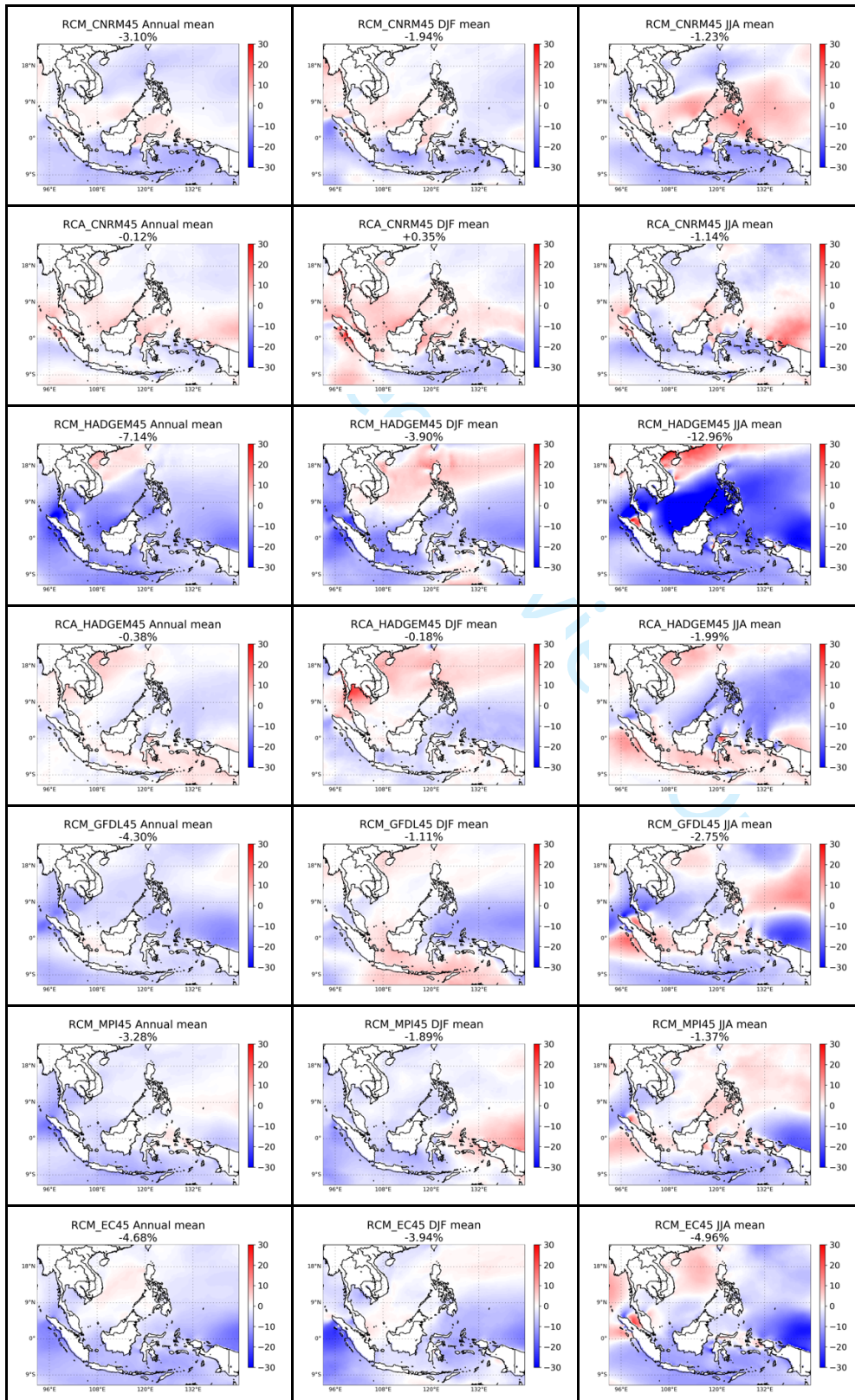
**Figure SM5. Same as Fig. SM1 for CVy.(%).**



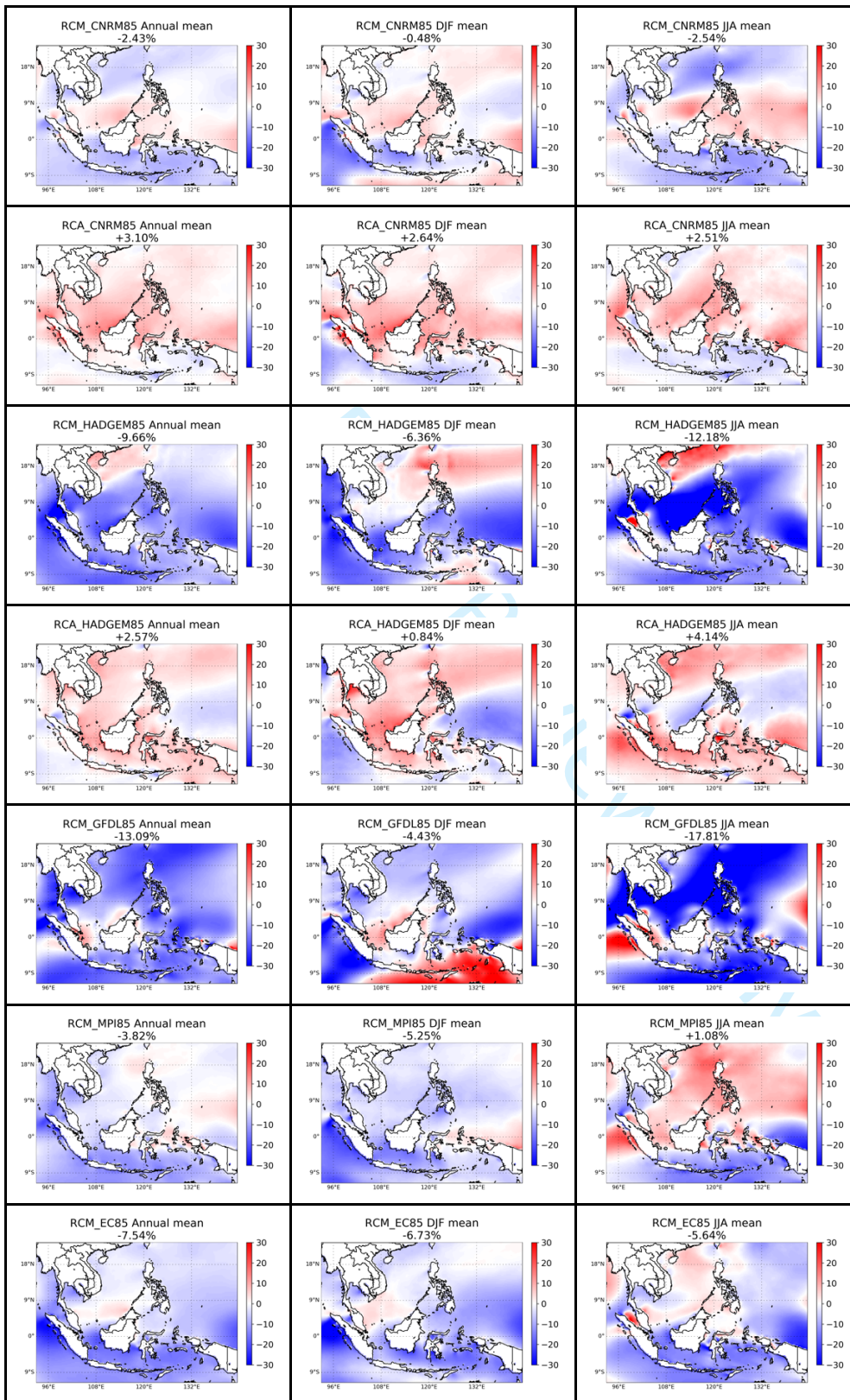
**Figure SM6. Same as Fig. SM5 for RCP8.5.**



**Figure SM7. Maps of the relative change (%) between the HIST and FUT periods of the average wind (m.s-1) for the whole year (left), DJF (middle) and JJA (right) for each of the 7 GCM\_RCM pairs in RCP4.5. Average value of average wind over the SEA and its relative variation between HIST and FUT are indicated in the titles.**



**Figure SM8. Same as Fig. SM7 for RCP85**



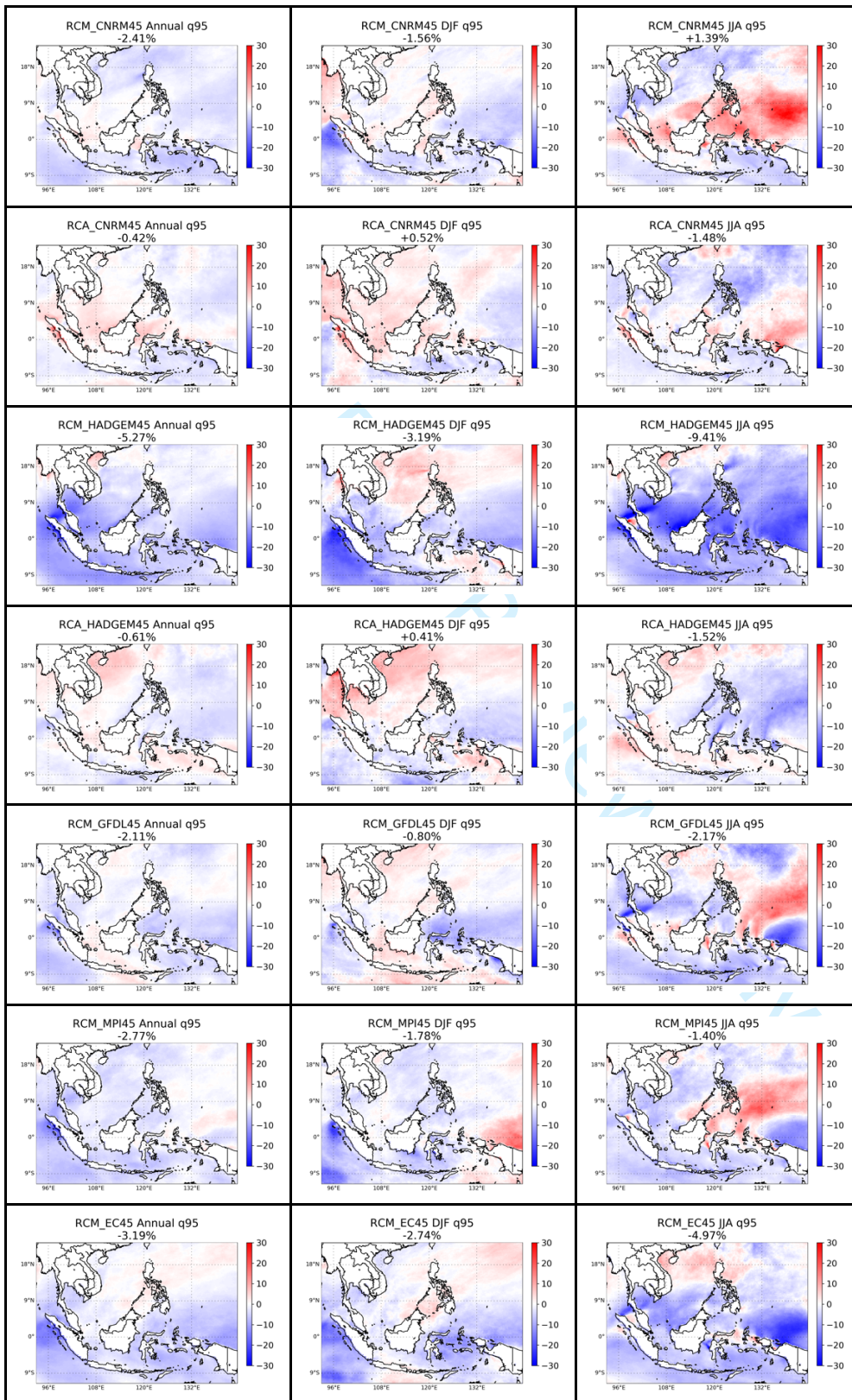
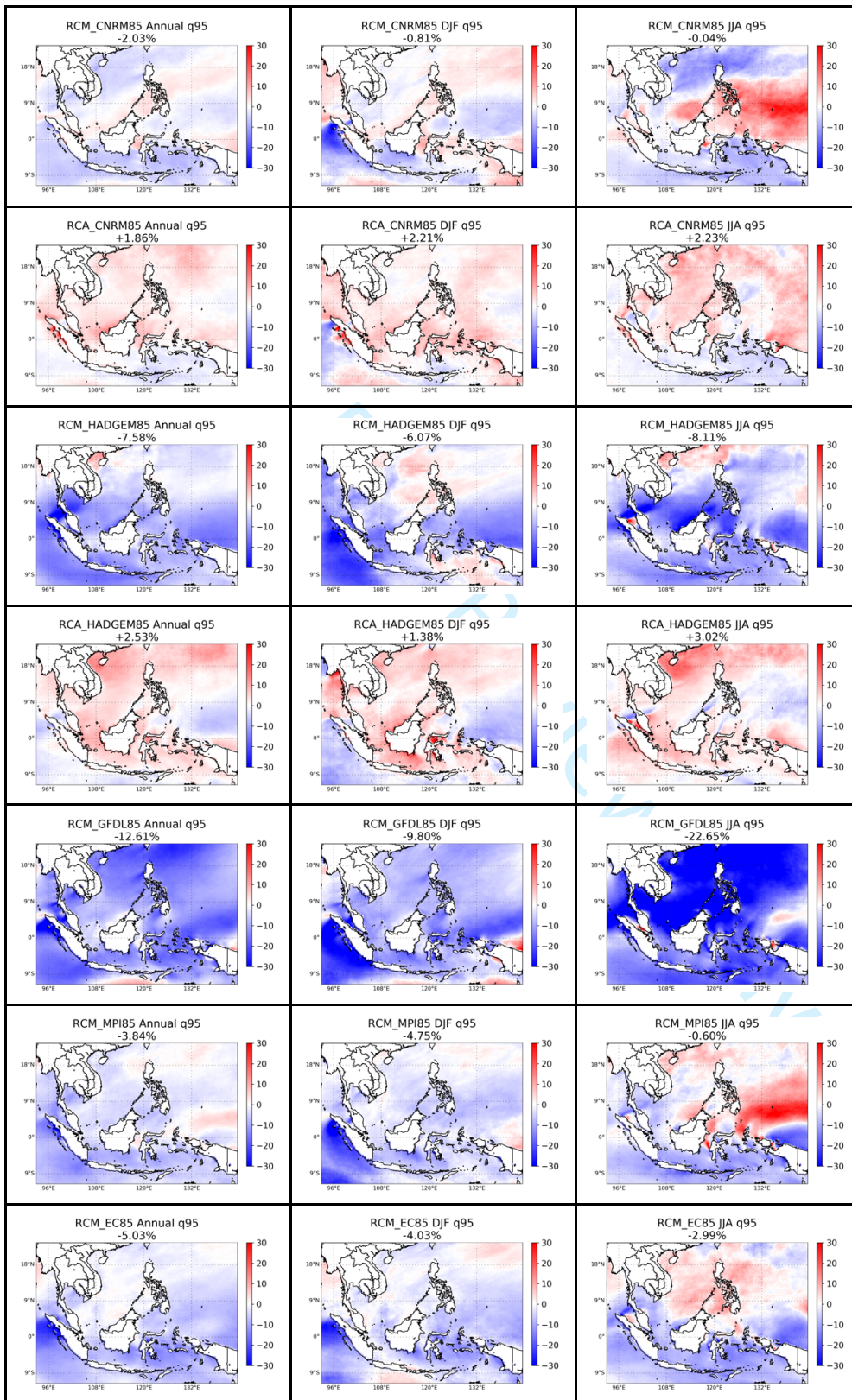
**Figure SM9. Same as Fig. SM7 for q95 (m.s-1).**

Figure SM10. Same as Fig. SM9 for RCP85.



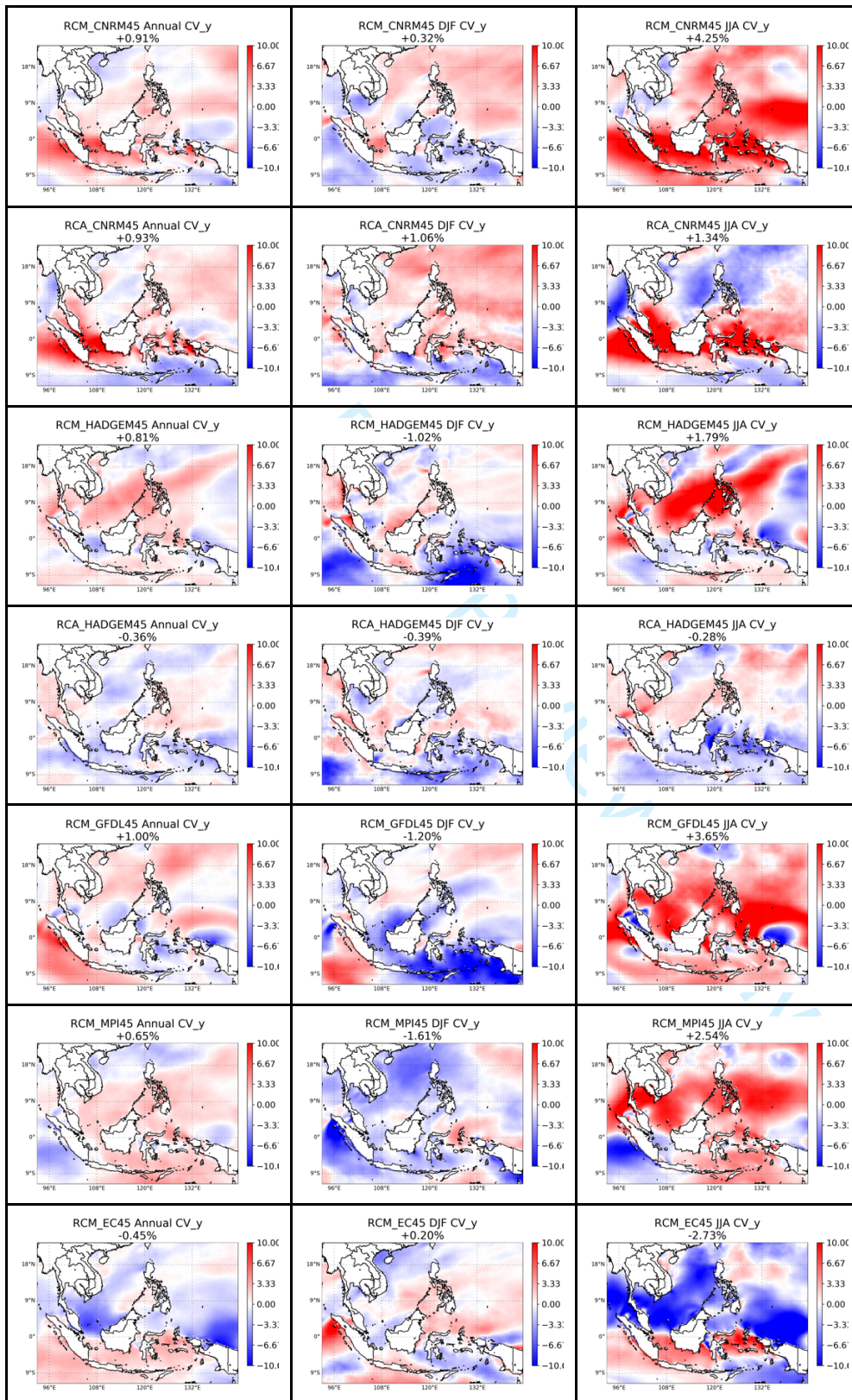
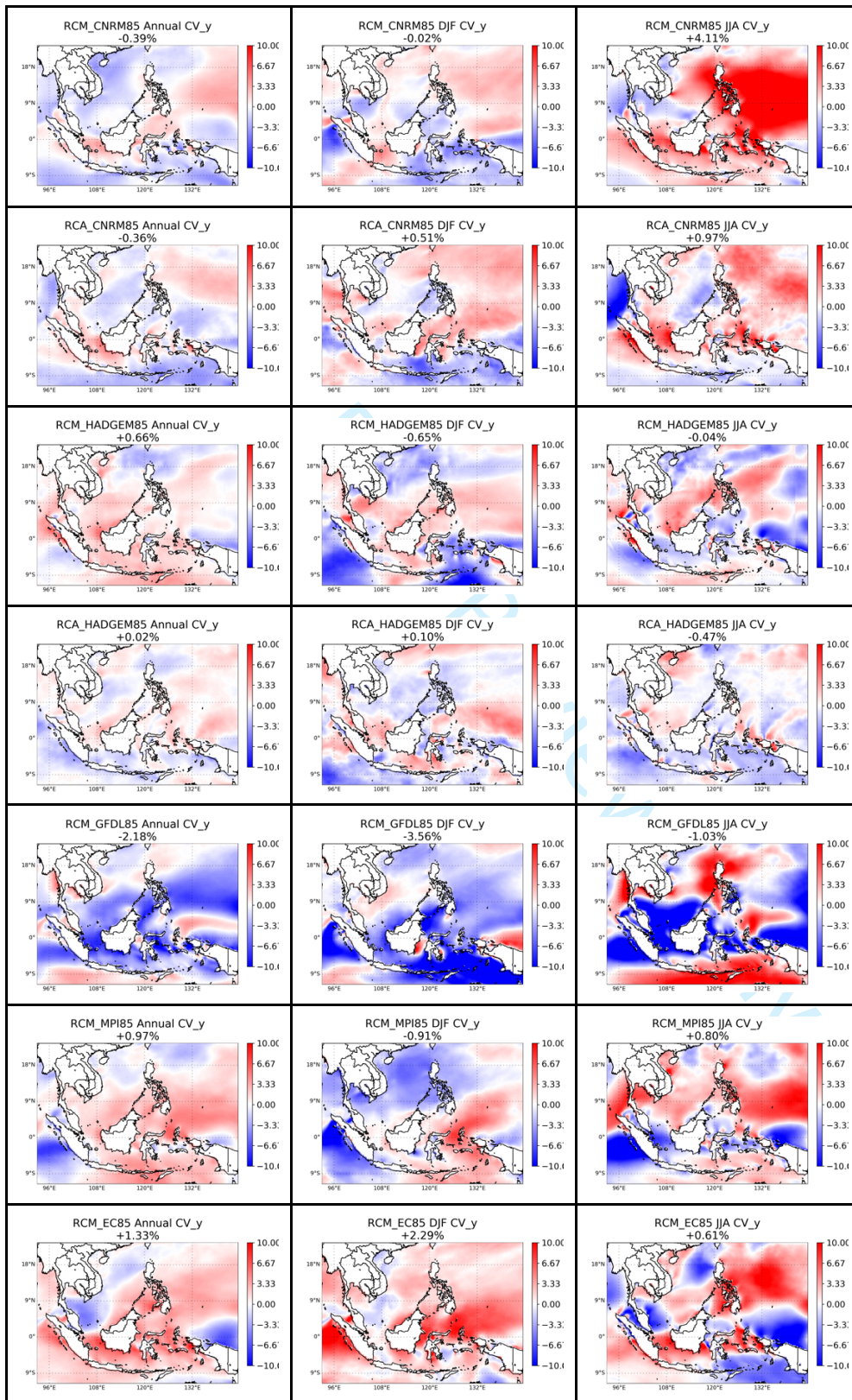
**Figure SM11. Same as Fig. SM7 for CVy (%).**

Figure SM12. Same as Fig. SM12 for RCP85



## **Climate change impact on sea surface winds in Southeast Asia**

**Marine Herrmann\*, Nguyen Duy Tung, Thanh Ngo-Duc, Fredolin Tangang**

Numerical representation and climate projections of sea surface winds over Southeast Asia are assessed here using an ensemble of downscaled simulations. Our results reveal significant differences in projections of sea surface wind, depending on the models, scenarios, regions and seasons. The only common signal is a weakening of summer seasonal and intense winds and an increase of seasonal wind interannual variability. Differences of seasonal sea surface wind changes between models are related to differences of sea level pressure gradient changes.

Peer Review Only

Relative change in sea surface wind speed between the end of 20th and 21st centuries

